land

MDPI

Article

Urban Expansion and Thermal Stress: A Remote Sensing Analysis of LULC and Urban Heat Islands in Ghaziabad, India

Mo Aqdas [1], Tariq Mahmood Usmani [1], Ramzi Benhizia [2] and György Szabó [2,*]

[1] Department of Geography, Aligarh Muslim University, Aligarh 202002, Uttar Pradesh, India; aqdasamu240@gmail.com (M.A.); tariqmahmoodusmani@gmail.com (T.M.U.)
[2] Department of Landscape Protection and Environmental Geography, University of Debrecen, Egyetem tér 1, 4032 Debrecen, Hungary; benhizia.ramzi@science.unideb.hu
* Correspondence: szabo.gyorgy@science.unideb.hu

Abstract

The climate and environment of metropolitan areas have been negatively impacted by swift urbanization and industrialization. Surface Urban Heat Islands (*SUHIs*) are among the most critical environmental phenomena. This research focused on the spatiotemporal analysis of land use/land cover (LULC) changes in relation to surface urban heat islands and their interconnections from 1992 to 2022. Land Surface Temperature (*LST*), LULC, and LULC indices, such as the Normalized Difference Moisture Index (*NDMI*), Normalized Difference Vegetation Index (*NDVI*), and Normalized Difference Built-up Index (*NDBI*), were generated using Landsat data. Urban hot spots (*UHSs*) were identified, and the Urban Thermal Field Variance Index (*UTFVI*) was then used to evaluate the spatiotemporal variation in thermal comfort. The results indicated *LST* values between a low of 14.24 and a maximum of 46.30. Urban areas and exposed surfaces, such as open or bare soil, exhibit the highest surface radiant temperatures. Conversely, regions characterized by vegetation and water bodies have the lowest. Additionally, this study explored the correlation between LULC, LULC indices, *LST*, and *SUHIs*. *LST* and *NDBI* show a positive relationship because of urbanization and industrialization (R^2 = 0.57 for the year 1992, R^2 = 0.38 for the year 2010, and R^2 = 0.35 for the year 2022), while *LST* shows an inverse relationship with *NDVI* and *NDMI*. Urban development should account for thermal sensitivity in densely populated regions. This study introduced an innovative spatiotemporal framework for monitoring long-term changes in urban surface environments. Furthermore, this research can assist planners in creating urban green spaces in cities of developing nations to minimize the adverse impacts of urban heat islands and improve thermal comfort.

Keywords: land use/land cover; land use indices; surface urban heat islands; thermal comfort; urban environment

check for updates

Academic Editor: Monika Kopecká

Received: 1 August 2025
Revised: 8 September 2025
Accepted: 13 September 2025
Published: 16 September 2025

Citation: Aqdas, M.; Usmani, T.M.; Benhizia, R.; Szabó, G. Urban Expansion and Thermal Stress: A Remote Sensing Analysis of LULC and Urban Heat Islands in Ghaziabad, India. *Land* **2025**, *14*, 1893. https://doi.org/10.3390/land14091893

Copyright: © 2025 by the authors. Licensee MDPI, Basel, Switzerland. This article is an open access article distributed under the terms and conditions of the Creative Commons Attribution (CC BY) license (https://creativecommons.org/licenses/by/4.0/).

1. Introduction

Urbanization refers to the migration of populations from rural to urban areas. Globally, urban populations have increased significantly over the past few decades, with estimates indicating that 55% of the world's population resided in urban areas in 2018—a figure projected to rise to 68% by 2050 [1]. Since independence, India has witnessed considerable urban expansion, driven largely by a rapidly growing urban population. The proportion of urban residents in India increased from approximately 17.3% in 1951 to 31.16% in 2011 [2]. It is projected that by 2030, over 40% of India's population will live in cities

and contribute to 75% of the country's GDP [3]. Urbanization, which involves both population migration to urban areas and land cover changes, has been strongly associated with environmental degradation, particularly in terms of waste generation, air pollution, and climate change [4,5]. The UHI effect is strongly linked to human-driven effects on energy consumption [6], air quality [7], and changes in precipitation patterns [8]. The UHI phenomenon, wherein the urban core experiences elevated temperatures compared to its surrounding suburban or rural areas [9,10], was initially observed by Luke Howard (1772–1864) [11]. Since then, numerous studies and literature reviews addressing the UHI phenomenon have been published shortly after their discovery, including literature reviews [12] and articles [13].

The recent surge in urban population is primarily attributed to extensive rural-to-urban migration, driven by enhanced economic opportunities and improved living conditions in cities and large metropolitan centers [14–16]. Urbanization transforms natural land into impervious surfaces, significantly changing its thermal characteristics and contributing to increased heat retention. These modifications intensify the thermal environment of urban areas and contribute to the formation of surface urban heat islands [17,18]. Understanding land use changes is essential for assessing the impacts of human activities on the landscape [19]. Changes in urban land use have led to several environmental issues, such as the emergence of localized microthermal and microclimatic zones [20]. Consequently, the decline in vegetation and the rapid growth of urban settlements are likely to elevate *LST* [21,22]. The integration of RS and GIS technologies has proven effective for modeling changes in LULC and *LST* [23–25].

UHIs are characterized by higher surface and air temperatures compared to their natural surroundings [26,27]. As a consequence of rapid urban expansion, significant LULC transformations have occurred in many cities. The most prominent consequence of LULC changes in Indian cities has been their impact on climate conditions, through rising temperatures, altered precipitation patterns, and declining air quality [20,28,29]. Several studies have quantitatively demonstrated a strong relationship between LULC changes and variations in land surface temperature [30–32].

The UHI effect can exacerbate extreme heat events, making them more intense and frequent [33,34]. Enhanced environmental pollution not only increases public health risks but also leads to higher energy consumption [35]. Urban heat islands (UHIs), air pollution, severe climatic conditions, and other human–nature conflicts are among the critical challenges that have arisen over the last century due to rapid urban expansion and LULC alterations [36]. Rapid urbanization and drastic land cover transformations have significantly altered surface energy balances, resulting in elevated land surface temperatures in urban centers [37]. Several studies have highlighted a strong association between *LST*, UHI intensity, and the spatial extent of built-up and vegetated areas [38–40]. The UHI effect leads to localized heat accumulation, resulting in higher urban temperatures relative to surrounding areas and posing serious health risks to urban populations [41,42]. The study of the UHI phenomenon is critical for developing effective thermal mitigation methods and improving the thermal resilience of urban environments, thereby contributing to the achievement of the United Nations Sustainable Development Goals [43]. Extreme temperatures observed on these high *LST* surfaces are referred to as urban hot spots [44]. Identifying and assessing *UHSs* is crucial for effective urban temperature regulation and maintaining ecological balance in the urban environment [45]. The main aim of this research is to identify urban hot spots within Ghaziabad, thereby assessing the prevailing levels of thermal comfort in the region.

Due to its proximity to the national capital, Ghaziabad has benefited from increased industrialization and associated economic opportunities. However, this rapid develop-

ment has also introduced significant environmental and infrastructural challenges. The city's thermal environment has experienced significant changes as a result of intensified industrial development and rapid urbanization. This research examines the dynamics of land use/land cover (LULC) and their interactions with land surface temperature (*LST*) and surface urban heat islands (*SUHIs*). Additionally, the study aims to identify urban hot spots and evaluate the correlations between different land use indices and *LST*. Unlike many previous remote sensing studies of urban heat islands, this research integrates *SUHIs* and *UTFVI* with UHS mapping to provide a more detailed assessment of thermal stress. By examining a three-decade period (1992–2022), it captures the long-term trajectory of UHI dynamics in Ghaziabad. The results of this investigation are expected to provide valuable insights into urban planning, environmental management, and the development of strategies aimed at mitigating the effects of climate change.

2. Materials and Methods

2.1. Study Area

Ghaziabad is located in the east of the national capital territory of Delhi and west of the state of Uttar Pradesh. It is in the National Capital Region (NCR), as shown in Figure 1. Due to its location adjacent to Delhi, it is known as the "Gateway of Uttar Pradesh." Ghaziabad is surrounded by the district Meerut in the north, Gautam Budh Nagar and Bulandshahar in the south, Hapur on the east, and the national capital Delhi on the west side. The city is divided into the CIS Hindon Area (CHA) in the east and the Trans-Hindon Area (THA) in the west by the Hindon River, which flows through it. THA comprises 1/3 of the city's area and population, while CHA comprises 2/3. Ghaziabad is a central industrial and corporate hub in Uttar Pradesh. In this area, similarly to other regions in northern India, there are mainly three distinct seasons: summer, winter, and the monsoon. The city experiences a dry and healthy climate, characterized by very high temperatures during the summer and significantly low temperatures in the winter. The monsoon season typically starts between late June and early July and continues until October. A significant amount of rainfall in the area occurs during the monsoon season. Ghaziabad, a significant district in Uttar Pradesh, is within the NCR and is part of the Meerut division. The 2011 census ranked it as the third-most populous district. Located in the center of the Ganga Yamuna doab, Ghaziabad has a roughly rectangular shape, measuring approximately 72 km in length and 37 km in width; the size of the sample area we examined is 177.9 km^2. Ghaziabad Metropolitan Area has a total population of 1,648,643, comprising 874,607 males and 774,036 females. Its geographical coordinates lie between 28°30′ and 28°59′ north latitude and 77°26′ and 78°10′ east longitude.

Different Landsat satellite images were used to assess LULC changes, extract *LST*, and examine UHI variations in the study area. All images featured a spatial resolution of 30 m for Bands 1–5 and 7 (Table 1). All Landsat images were sourced from the United States Geological Survey (USGS) platform (https://earthexplorer.usgs.gov/, accessed on 12 October 2024). These datasets are widely used for surface temperature estimations [46] and LULC change assessments [47]. The selected images had high spatial resolution and cloud cover of less than 2%. The shapefile for the study area was obtained from a verified source. Georeferencing was initially conducted using four Ground Control Points (GCPs), followed by careful digitization of the shapefile.

To investigate changes in LULC, *LST*, and *NDVI* within Ghaziabad, all data were transformed into the UTM/WGS84 coordinate system. Landsat images were geometrically corrected to the Zone 43 North UTM projection using the WGS84 geodetic datum. ArcGIS 10.8 software (Esri, Redlands, CA, USA) was utilized for spatial analysis, while ERDAS 2014 (Hexagon Geospatial, Sweden) was employed to assess LULC changes and process images.

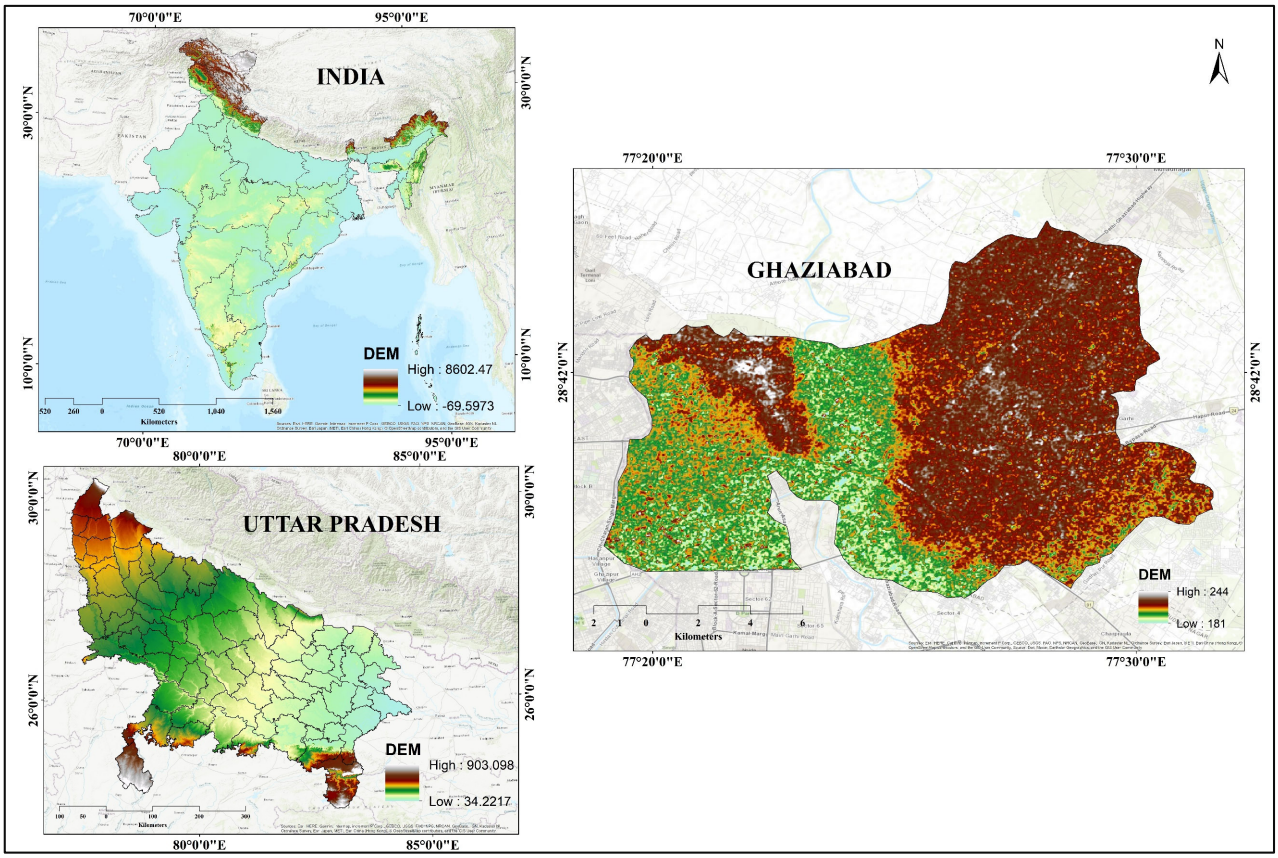

Figure 1. Geographical location of the study area.

Table 1. Satellite datasets utilized for the study.

Sr. No	Satellite/Sensor	Acquisition Date	Cloud Cover (%)	Path/Row	Spatial Resolution of Spectral Bands (m)
1	Landsat 5 TM	16 March 1992	10.00	146/40	30
2	Landsat 5 TM	3 April 2010	0.01	146/40	30
3	Landsat 8	4 April 2022	0.00	146/40	30

2.2. Image Processing and Classification

The study area was delineated, and false color composite (FCC) images were generated by combining spectral bands to facilitate visual interpretation and improve classification accuracy. Visual interpretation provides valuable insights into land cover changes over time [48]. Image enhancement techniques have improved the interpretability of satellite imagery [49].

Remote sensing techniques employing Landsat images have been used to classify and map LULC changes by identifying distinct landscape elements [50]. More than 300 training samples were collected across all LULC classes to ensure accurate classification, with over 70 samples collected for each class. Five LULC categories were identified to assess the impact of land use changes on *LST* and *SUHIs*.

These categories—built-up area, agriculture, open land, vegetation, and water bodies—were classified using a supervised approach. The maximum likelihood algorithm was employed to classify the five land cover categories. The thermal band was excluded due to its non-reflective properties [49]. A detailed description of LULC classes is given in Table 2.

Table 2. Description of various LULC classes.

LULC Class	Details of the LULC Class
Built-Up Area	Includes all residential, business, and industrial areas, settlements, villages, and infrastructure related to transportation.
Vegetation	Comprises natural forest, trees, shrubs, and all types of vegetation (excluding standing crops).
Agriculture	Encompasses cropland, including both large and small farms, as well as mechanized farms.
Water Bodies	Refers to anybody of open water, such as ponds, rivers, and lakes.
Open Land	Areas devoid of vegetation of vegetation are mainly made up of bare earth, exposed soil, and other natural rock surfaces.

2.3. Land Use/Land Cover (LULC) Extraction and Change Analysis

There are several ways to implement supervised classification; however, in this study, the commonly used maximum likelihood classifier (MLC) was employed together with ERDAS IMAGINE software. Ghaziabad was classified into five main LULC classes—built-up area, vegetation, agricultural, open land, and water bodies. Different spectral signatures of Landsat images were identified and validated using Google Earth images from the same period. Before assigning LULC classifications, band composition was applied to the Landsat images. The maximum likelihood classifier was applied using composite bands from the three study years as input parameters; a critical advantage of parametric algorithms, such as MLC, is their ease of application. Parametric techniques are especially effective for less complex terrains with well-defined LULC categories

Producer Accuracy (PA) measures the percentage of correctly classified pixels for a given class. In contrast, User Accuracy (UA) indicates the likelihood that a pixel classified as a particular category genuinely belongs to that category. The ratio of the accurately classified reference points to the total reference points was considered to calculate the overall accuracy.

2.4. Accuracy Assessment

Accuracy can be assessed by comparing reference data with information obtained through remote sensing techniques [51,52], emphasizing the importance of the number and representativeness of training samples in image classification. Additionally, it is vital to collect ground reference data as close as possible to the date of the historical imagery [53]. Ref. [54] notes that reference data were systematically generated for accurate evaluation. Ref. [55] reported using a stratified random sampling method to generate reference points for accuracy assessment. They also noted that a confusion matrix was employed to evaluate the accuracy of each LULC map [56]. A confusion matrix was generated in ERDAS IMAGINE 2014 to compute user accuracy, producer accuracy, and overall classification accuracy. The outcomes and confusion matrix for various LULC classifications are presented in Table 3. The overall accuracy of the LULC maps is above 90%.

Table 3. User's accuracy, producer's accuracy, and overall accuracy assessment of land use/land cover classification: 1992–2022.

LULC CLASS	1992			2010			2022		
	UA	PA	OA	UA	PA	OA	UA	PA	OA
Built-Up Area	98.65	97.95		100	93.57		99.92	98.34	
Vegetation	93.07	96.58		96.56	96.98		99.12	97.19	
Agriculture	87.66	83.85	95.40	67.808	85.34	93.27	88.30	98.28	98.16
Open Land	91.86	88.76		75.21	95.65		100	100	
Water Bodies	94.78	99.09		83.89	88.39		100	99.10	

2.5. Derivation of Spectral Indices

2.5.1. Normalized Difference Vegetation Index (*NDVI*)

The *NDVI* is an indicator of relative greenness used to assess vegetation. It is also effective for monitoring vegetation productivity and identifying changes in vegetation [57]. Surfaces without vegetation exhibited negative values [58]. *NDVI* analysis was conducted using ArcGIS 10.8 to identify green areas within Ghaziabad and to validate land use changes detected from satellite imagery. The required bands were added in ArcGIS, and the calculation was performed using a raster calculator. *NDVI* was calculated as suggested by [59] using Equation (1).

$$NDVI = \frac{NIR - R}{NIR + R} \quad (1)$$

Whereas *R* corresponds to band 3 in Landsat 5 (TM), it represents band 4 in Landsat 8 OLI and TIRS. On the other hand, *NIR* signifies band 4 in Landsat 5 TM and band 5 in Landsat 8.

2.5.2. Normalized Difference Built-Up Index (*NDBI*)

Previous studies have shown that high *NDBI* values indicate urbanized areas, whereas negative values represent non-urban features such as vegetation and water bodies [60]. In urban settings and exposed soil, reflectance in the Short-Wave Infrared (SWIR) spectrum exceeds that of the Near Infrared (NIR). The infrared spectrum did not reflect water bodies. *NDBI* is determined using reflectance values from the SWIR and NIR bands in remote sensing data. *NDBI* values vary from −1 to +1, with negative values indicating water bodies and higher values signifying built-up areas. Vegetation typically exhibits low *NDBI* values.

NDBI was estimated using the method described by [60] using Equation (2).

$$NDBI = \frac{NIR - SWIR}{NIR + SWIR} \quad (2)$$

Band 5 in Landsat 5 (TM) and band 6 in Landsat 8 (OLI/TIRS) correspond to the *SWIR* band.

2.5.3. Normalized Difference Moisture Index (*NDMI*)

NDMI was derived by computing the normalized difference between the NIR and SWIR bands. It indicates the moisture content of vegetation and assesses the water stress level. By analyzing the *NDMI*'s absolute value, it is possible to pinpoint areas of a field or farm experiencing water stress.

As suggested by [61], the NIR and SWIR bands were used to calculate the *NDMI*. The calculation was performed using Equation (3).

$$NDMI = \frac{NIR - SWIR}{NIR + SWIR} \quad (3)$$

The information regarding bands is mentioned above.

2.6. Retrieval of Land Surface Temperature (LST)

LST was computed over three years using thermal bands from Landsat satellite imagery. ArcGIS 10.8 software was used to retrieve *LST*. The *LST* retrieval process involved three main steps: (i) determining the brightness temperature, (ii) estimating the amount of vegetation (*Pv*), and (iii) correcting emissivity using *NDVI* [62]. This is among the most widely used methods that differentiates between vegetated and non-vegetated areas. It is also used in the areas of mixed land cover, where emissivity varies significantly. The entire *LST* retrieval methodology for the different Landsat sensors is described below.

2.6.1. Retrieval of LST for Landsat 5 (TM)

Step 1: Top of Atmospheric Radiance

The equation suggested by Artis and Carnahan was used to calculate spectral radiance, as shown in Equation (4).

$$L\lambda = \left\{ \frac{L_{MAX}\lambda - L_{MIN}\lambda}{Qcal_{MAX} - Qcal_{MIN}} \right\} (Qcal - Qcal_{MIN}) + L_{MIN}\lambda \quad (4)$$

where $L\lambda$ stands for spectral radiance; L_{MAX} λ for the maximum spectral radiance of the satellite sensor, scaled to correspond with the maximum quantized calibration value ($Qcal_{MAX}$); and L_{MIN} λ for the minimum spectral radiance of the satellite sensor, scaled to match the minimum quantized calibration value ($Qcal_{MIN}$).

Step 2: Convert Radiance into Brightness Temperature (BT) in Kelvin

The next step involved applying Equation (5) to calculate the brightness temperature (BT) from the top of the atmosphere (TOA) reflectance [63].

$$BT = \left\{ \frac{K2}{\mathrm{Ln}\left(\frac{K1}{L\lambda} + 1\right)} \right\} \quad (5)$$

In the above equation, $L\lambda$ represents spectral radiance, and BT represents brightness temperature expressed in Kelvin. The constants $K1$ and $K2$ are radiometric calibration parameters provided in Table 4.

Table 4. K values of thermal bands of Landsat satellites.

Sr. No	Satellite/Sensor	Thermal Band	*K1*	*K2*
1	Landsat 5 TM	6	607.76	1260.56
2	Landsat 8 OLI/TIRS	10	774.8853	1321.07

Step 3: Conversion of Kelvin into Degrees Celsius

The temperature values were converted from Kelvin to degrees Celsius using the following Equation (6).

$$T(^{\circ}\mathrm{C}) = BT - 273.15 \quad (6)$$

In this equation, $T(^{\circ}\mathrm{C})$ refers to Land Surface Temperature, and BT is the measured temperature in Kelvin.

2.6.2. Extracting *LST* from Landsat 8 Data

(i) Top of Atmosphere (TOA) Radiance

The radiance rescaling factor transforms thermal infrared digital numbers into Top-of-Atmosphere (TOA) spectral radiance, as shown in Equation (7).

$$L\lambda = M_L \times Qcal + A_L \quad (7)$$

$L\lambda$ represents TOA spectral radiance, expressed in watts per square meter per steradian per micrometer ($\mathrm{W{\cdot}m^{-2}{\cdot}sr^{-1}{\cdot}\mu m^{-1}}$). $Qcal$ represents the pixel's quantized and calibrated DN values in the standard product. M_L is the radiance multiplicative scaling factor for the particular band, while A_L is the corresponding additive factor.

(ii) Conversion of Top of Atmosphere (TOA)/Brightness Temperature (BT)

Thermal calibration constants from the Metadata file were used to convert spectral radiance data into top-of-atmosphere brightness temperature, as shown in Equation (8).

$$\mathrm{BT} = \left\{ \frac{K2}{\mathrm{Ln}\left(\frac{K1}{L\lambda} + 1\right)} \right\} \tag{8}$$

BT is the brightness temperature at the top of the atmosphere, measured in Kelvin $L\lambda$ is the is the top-of-atmosphere spectral radiance, measured in watts per square meter per steradian per micrometer {W/ ($m^2 \times r \times \mu m$)}. *K1* and *K2* are constants specific to the bands being evaluated.

(iii) Normalized Differential Vegetation Index (NDVI)

NDVI has been calculated as previously described in Equation (1).

(iv) Proportion of Vegetation Index

The proportion of vegetation (*Pv*) was calculated using Equation (9).

$$Pv = \left\{ \frac{NDVI - NDVI_{min}}{NDVI_{max} + NDVI_{min}} \right\}^2 \tag{9}$$

In this context, *PV* is the proportion of vegetation, *NDVI* is the DN value from the *NDVI* image, and $NDVI_{min}$ and $NDVI_{max}$ are the minimum and maximum DN values from the *NDVI* image, respectively.

(v) Land Surface Emissivity (LSE):

LSE is a parameter that describes the average emissivity of the earth's surface, as determined by *NDVI* values, and is based on the radiative properties of natural land features. It is calculated by using Equation (10).

$$E = 0.004\ Pv + 0.986 \tag{10}$$

P_V represents the vegetation proportion, and E stands for land surface emissivity.

(vi) Land Surface Temperature (LST)

The radiative temperature, known as *LST*, was estimated by utilizing the wavelength of the emitted radiation, land surface emissivity, and brightness temperature at the top of the atmosphere, as shown in Equation (11).

$$LST = \left[\frac{BT}{1 + \left(\lambda \times \frac{BT}{\rho}\right) ln(E)} \right] - 273.15 \tag{11}$$

BT is the brightness temperature measured in Kelvin, λ is the wavelength of the emitted radiation, *E* denotes land surface emissivity, and the ρ value is 14,380.

2.7. Estimation of Surface Urban Heat Islands (SUHIs)

UHI represents a prominent environmental issue that impacts major cities where the air temperature is considerably higher than in surrounding suburban areas. The UHI effect also contributes to poor air quality and atmospheric haze. High-density urban infrastructures significantly contribute to the UHI effect since they not only restrict airflow but also release heat from solar energy that has been captured. The loss of wetlands and vegetation further reduces the ability of cities to release heat. Since the UHI impact poses a serious concern to the environment and human health [64,65], minimizing and mitigating it has become essential. *SUHIs* have been used in numerous prior studies to investigate the spatial extent and intensity of UHIs [66–69].

The surface urban heat island (*SUHI*) was calculated by using Equation (12).

$$SUHI = \left[\frac{\{Ts - Tmean\}}{SD} \right] \tag{12}$$

In this equation, *Tmean* is the mean *LST*, *SD* is the standard deviation of *LST*; *Ts* is the *LST* at a specific location.

2.8. Modeling of Urban Hot Spots (UHSs)

The UHS was modeled to identify areas with the highest land surface temperatures (*LST*). UHS typically occurs in isolated areas of highly densely populated land, barren land, or open land that manifests unusually hot temperatures and is unsuitable for human habitation. The *UHSs* were modeled using Equation (13), following the method of [45].

$$UHS = [LST > \mu + 2 \times \delta] \quad (13)$$

In this equation, μ denotes the mean *LST*, while δ is the standard deviation of *LST* within the study area.

2.9. Estimation of UTFVI

The Urban Thermal Field Variance Index (*UTFVI*) is an extensively used metric for quantifying the surface urban heat island effect [70]. *UTFVI* values are typically higher and concentrated in areas experiencing elevated surface temperatures compared to their surrounding environments [71]. This index categorizes Ghaziabad into six thermal ecological zones: excellent, good, normal, bad, worse, and worst, based on levels of human thermal comfort. These categories represent a gradient of thermal conditions, ranging from optimal to severely uncomfortable [72]. Equation (14) was used to model the *UTFVI* [73].

$$UTFVI = \left[\frac{\{Ts - Tmean\}}{Tmean}\right] \quad (14)$$

The comprehensive methodology is shown in Figure 2.

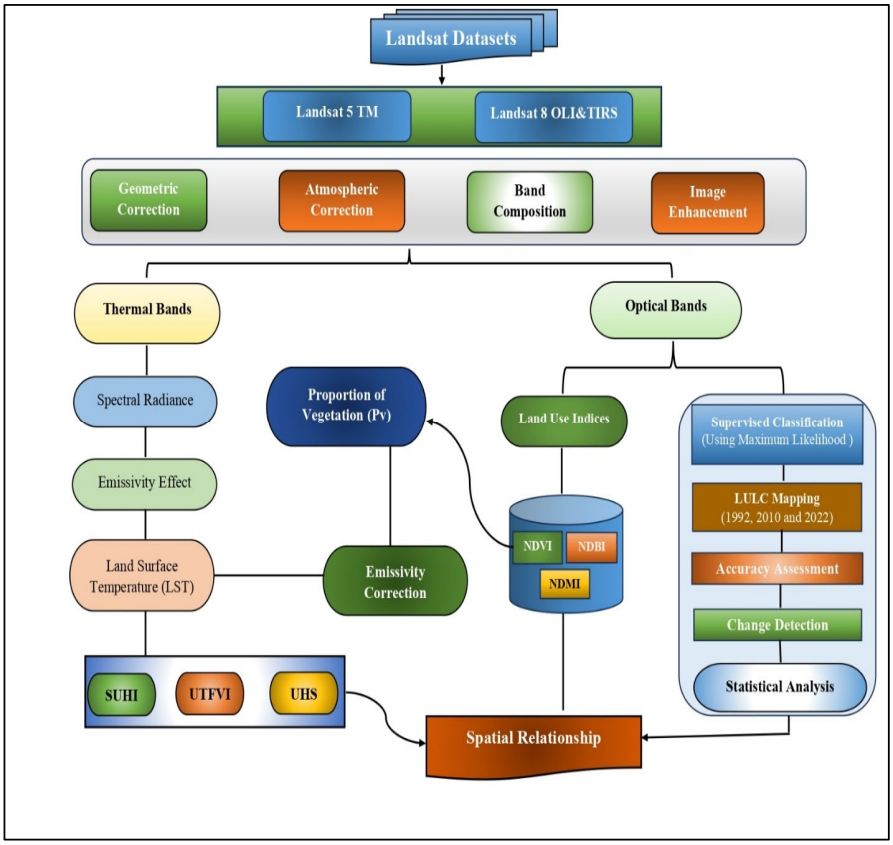

Figure 2. Workflow chart of the methodology.

3. Results

3.1. Land Use/Land Cover Dynamics: Unveiling the Changes

LULC dynamics play a crucial role in shaping the ecosystem. The state of the natural environment is closely tied to LULC, as changes in land use directly affect the natural environment and contribute to broader climate change phenomena, consequently worsening public health concerns. The ongoing process of LULC change is shaped by various factors, including socioeconomic conditions, political influences, cultural aspects, demographic trends, and environmental considerations [74]. To investigate the spatiotemporal development of urban heat in connection with urbanization, the study was conducted for the years 1992, 2010, and 2022. Analyzing UHIs and their relationship with urban expansion helps to identify climate and environmental vulnerabilities in urban areas. The analysis focused on Ghaziabad in Uttar Pradesh. While Ghaziabad has experienced rapid urbanization, the city's growth rate remains relatively high, at 70.22%, as depicted in Figure 3 [75].

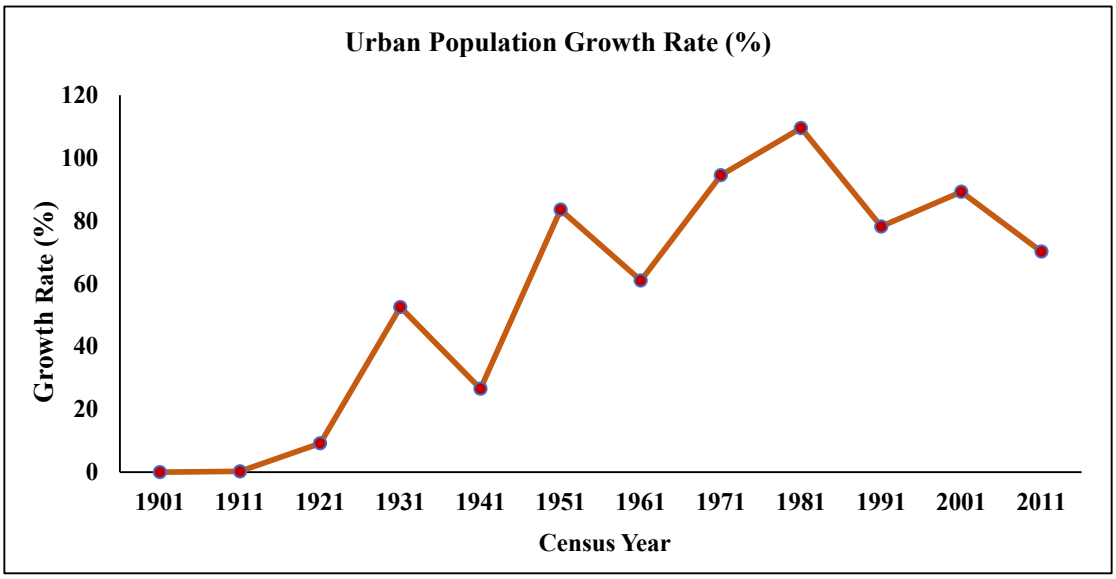

Figure 3. Urban population growth rate of Ghaziabad Urban Agglomeration from 1901 to 2011.

Figure 4 presents the supervised LULC classification. Three land use maps for 1992–2022 were created using supervised classification and post-classification techniques on Landsat data. In 1992, agricultural land covered 52.52 sq. km (28.38%); built-up area, 53.64 sq. km (29.01%); vegetation, 47.61 sq. km (26.74%); open land, 24.8 sq. km (13.9%), and water bodies, 3.39 sq. km (1.90%) (Table 5). The built-up areas in Ghaziabad were primarily found in the southwest, south, and central regions. The northeastern and riverbank regions of Ghaziabad were primarily covered by vegetation. Small pockets of open ground were found in Ghaziabad's southern and northern regions.

The LULC trends recorded in Ghaziabad between 1992 and 2010 are shown in Table 5. There was a 9.42% increase in the built-up areas. In contrast, all classes, including vegetation, water bodies, and open land, showed declines of −22.08%, −0.35%, and −1.7%, respectively. This demonstrates that vegetation was the most adversely impacted land use category. The primary cause of these declines was the ongoing expansion of both agricultural and downtown areas, and an increase in population, housing demand, and agricultural development, which has turned open lands and natural vegetation into urban and agricultural zones.

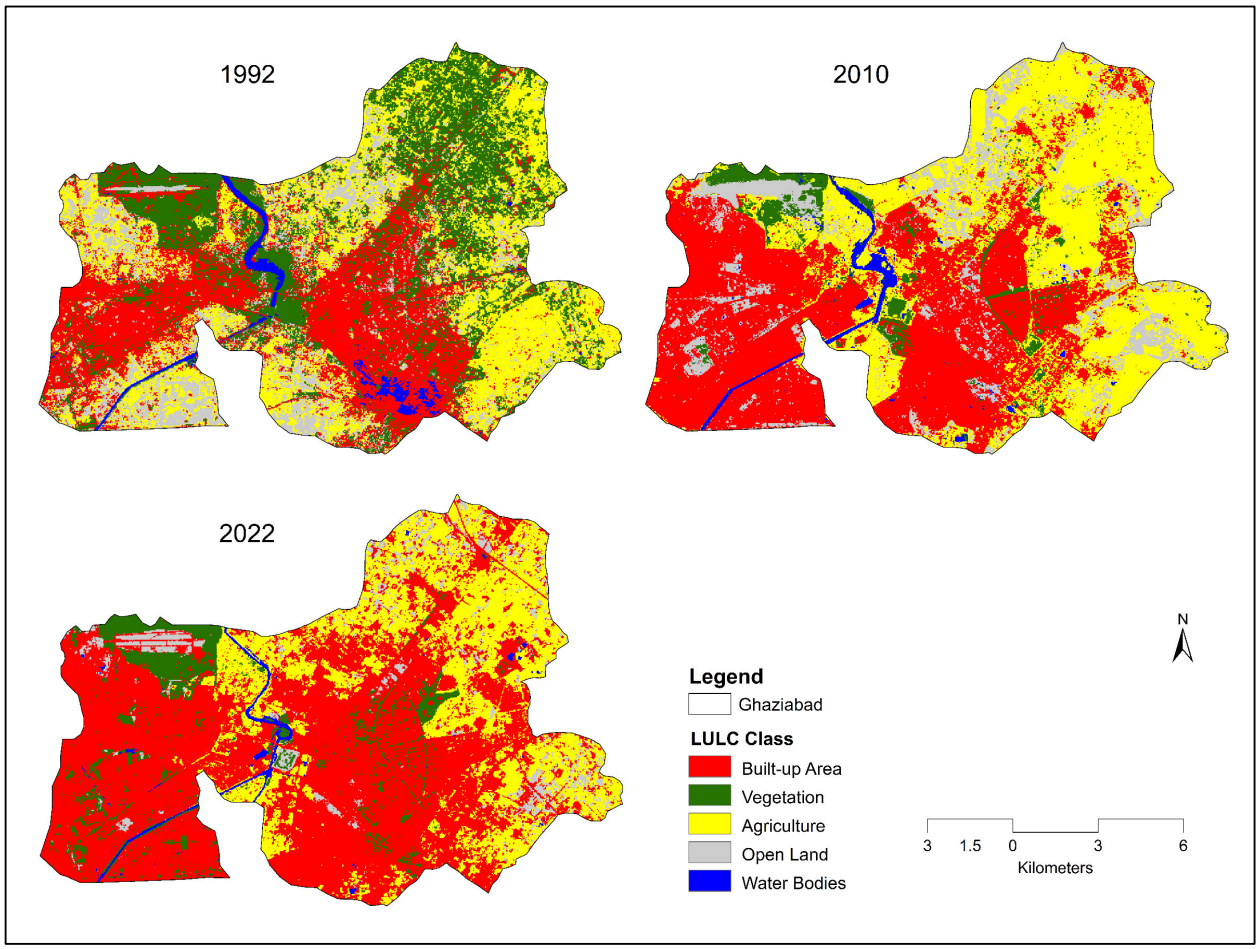

Figure 4. Graphical representation of different LULC classes for different time periods.

Table 5. Changes in land use/land cover for different classes in Ghaziabad: 1992–2022.

LULC Class	(1992). Area (km^2)	1992 (%)	2010 Area (km^2)	2010 (%)	2022 Area (km^2)	2022 (%)	% Change (1992–2010)	% Change (2010–2022)	% Change (1992–2022)
Agriculture	52.52	28.38	66	37.8	49.45	27.78	9.42	–10.02	–0.60
Built-up Area	51.64	29.01	79.17	44.48	106.3	59.76	15.47	15.28	30.75
Vegetation	47.61	26.74	8.29	4.66	11.65	6.55	–22.08	1.89	–20.19
Water Bodies	3.39	1.9	2.77	1.55	1.9	1.06	–0.35	–0.49	–0.84
Open Land	24.8	13.9	21.72	12.2	8.6	4.83	–1.70	–7.37	–9.07
Total Area	177.9		177.9		177.9				

Table 5 shows the patterns and areas of various LULC classes for 2022. Built-up areas are the only category that has consistently increased. This contributed 59.76 percent. Its area increased from 79.17 sq km in 2010 to 106.30 sq km in 2022, as presented in Figures 5 and 6. Except for a slight increase in vegetation, all other land use categories showed a decline by 2022. Over the whole study period, four of the LULC classes—vegetation, water bodies, open land, and agriculture—have observed significant declines of −20.19%, −0.84%, −9.07%, and −0.6%, respectively, while built-up areas have increased (+30.75).

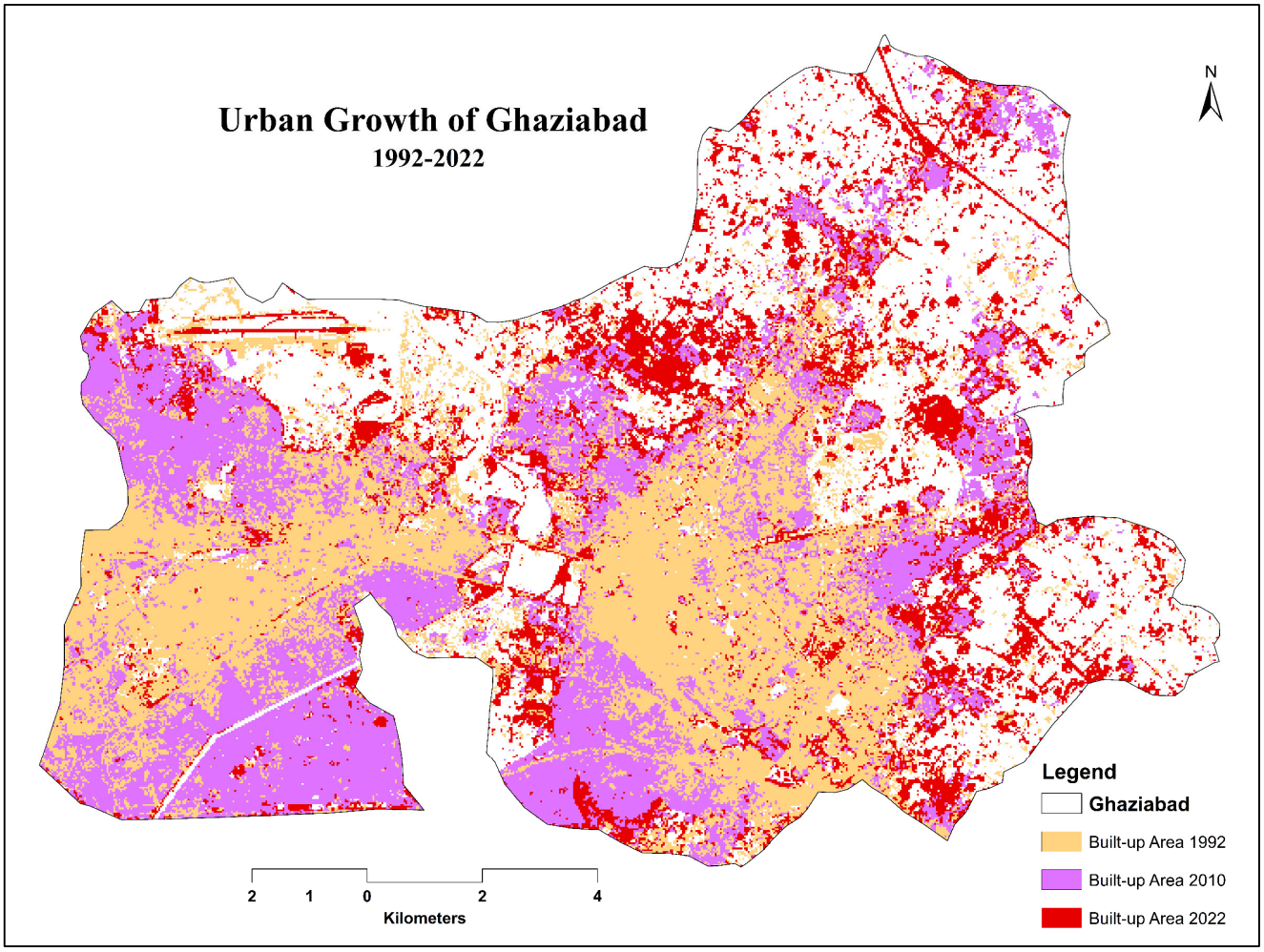

Figure 5. Urban growth of Ghaziabad: 1992–2022.

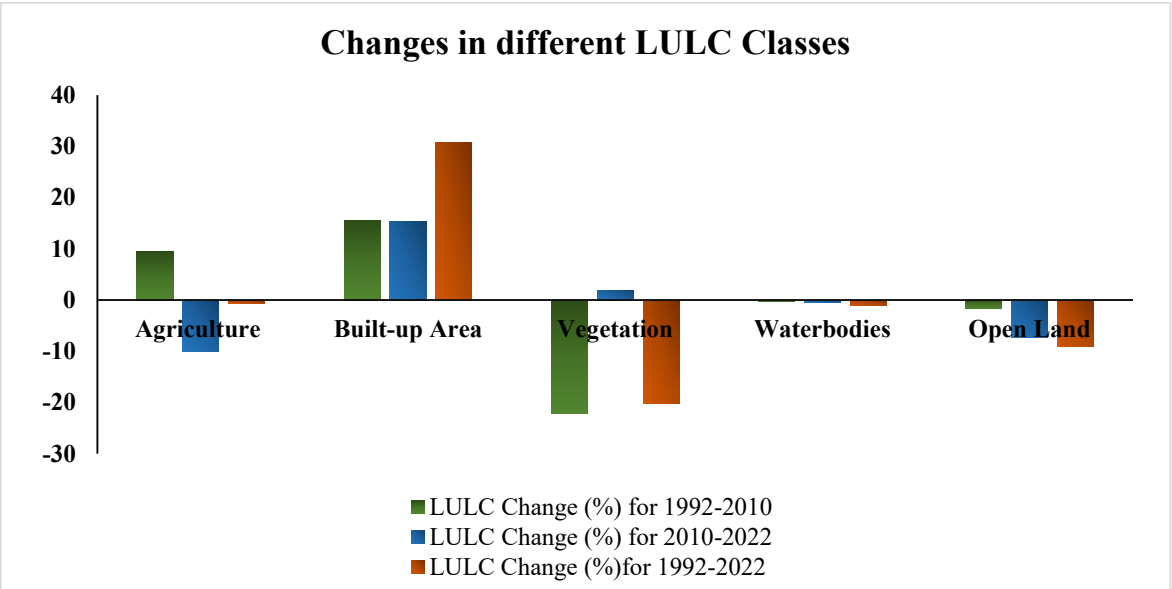

Figure 6. Graphical representation of changes in various LULC classes, in percentage.

3.2. Transformation of Land Use/Land Cover (1992–2022)

Land use/land cover (LULC) in Ghaziabad experienced significant changes between 1992 and 2022, as shown in Table 5 and Figure 7. This indicates that the built-up area grew

steadily for all three periods: 1992, 2010, and 2022. The built-up area recorded a consistent growth across the three study periods, increasing from 53.64 sq. km (29.01%) in 1992 to 79.17 sq. km (44.48%) in 2010, and further to 106.30 sq. km (59.76%) in 2022, with a total positive change of 30.75%. This represents the most significant increase among all LULC categories. However, during the same period, there was a decline in agricultural land (−0.60%), vegetation (−20.19%), water bodies (−0.84%), and open land (−9.7%). Among these, vegetation experienced the most significant decline.

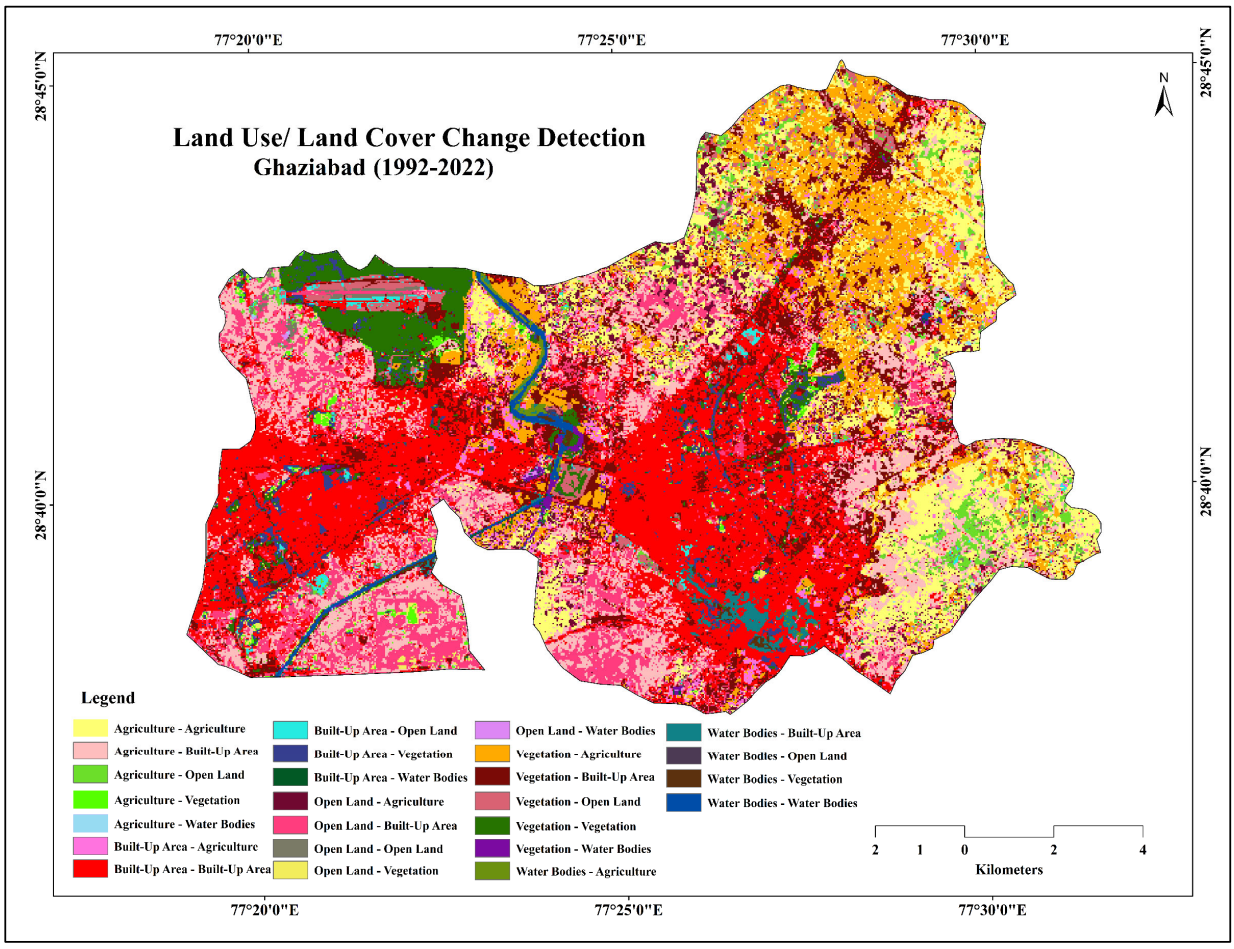

Figure 7. Land Use/ Land Cover change detection in Ghaziabad: 1992–2022.

Temporally, built-up areas increased from 29.01% in 1992 to 44.48% in 2010 and 59.76% in 2022, as shown in Figure 4. A downward tendency in open land was observed: from 13.90% in 1992 to 12.20% in 2010, then to just 4.83% in 2022. Additionally, vegetation cover declined from 26.74% in 1992 to 4.66% in 2010, followed by a slight increase to 6.55% in 2022. Water bodies also experienced a decline, from 1.90% in 1992 to 1.55% in 2010, and further to 1.06% in 2022. Anthropogenic influences were primarily responsible for this decline, including urbanization and infrastructure expansion. Moreover, agricultural land increased from 28.38% in 1992 to 37.80% in 2010, but declined again to 27.78% by 2022. The growth of urban settlements between 2010 and 2022 was a significant factor in the decline in agriculture.

Figure 4 shows the spatiotemporal dynamics of LULC in Ghaziabad in 1992, 2010, and 2022. Vegetation in the northeastern part in 1992 was transformed mainly into agricultural and built-up areas by 2022. Meanwhile, open land has also decreased continuously from 1992 to 2022. The built-up area has experienced a significant increase during the study period, as illustrated in Figure 5. Agriculture is mainly distributed in the surrounding areas.

Its predominance was on the eastern and northeastern sides. Water bodies appear to have decreased from 1992 to 2022. Most built-up areas were converted from open vegetation and agricultural land.

Figure 6 provides a clear and accessible visualization of LULC changes between 1992 and 2010; vegetation was substantially converted into agricultural land and open areas, as shown in Figure 6. Meanwhile, the LULC class showed a slight recovery between 2010 and 2022. The built-up area was the only category that grew consistently during the study period. Owing to the transformation of the majority of vegetation into agricultural land, there was an increase in agricultural land from 1992 to 2010. The water bodies consistently shrank during the study period. The amount of open land steadily decreased throughout the study period. Open land is also a key factor for the high *LST* in built-up areas. Contributing to elevated *LST* in built-up areas, exacerbating the formation of UHIs in Ghaziabad. Figure 7 presents a more detailed representation of LULC change detection.

3.3. Spatiotemporal Analysis of Spectral Indices in Ghaziabad: 1992–2022

3.3.1. Spatiotemporal Analysis of Normalized Difference Vegetation Index (*NDVI*) in Ghaziabad: 1992–2022

The spatial distribution of *NDVI* values across Ghaziabad is illustrated in Figure 8. The *NDVI* values range from −0.13 to 0.63, −0.11 to 0.51, and 0.03 to 0.49 in 1992, 2010, and 2022, respectively, as shown in Table 6. In 1992, higher *NDVI* values were primarily associated with areas of dense vegetation and active agricultural practices, particularly in the northeastern and eastern regions. In contrast, in 2010 and 2022, increased *NDVI* values were more distinctly observed along riverbanks and surrounding Hindon Airport. The *NDVI* values are closely linked to LULC, with the highest values observed over vegetation and agricultural areas and the lowest values over built-up areas, open land, and water bodies.

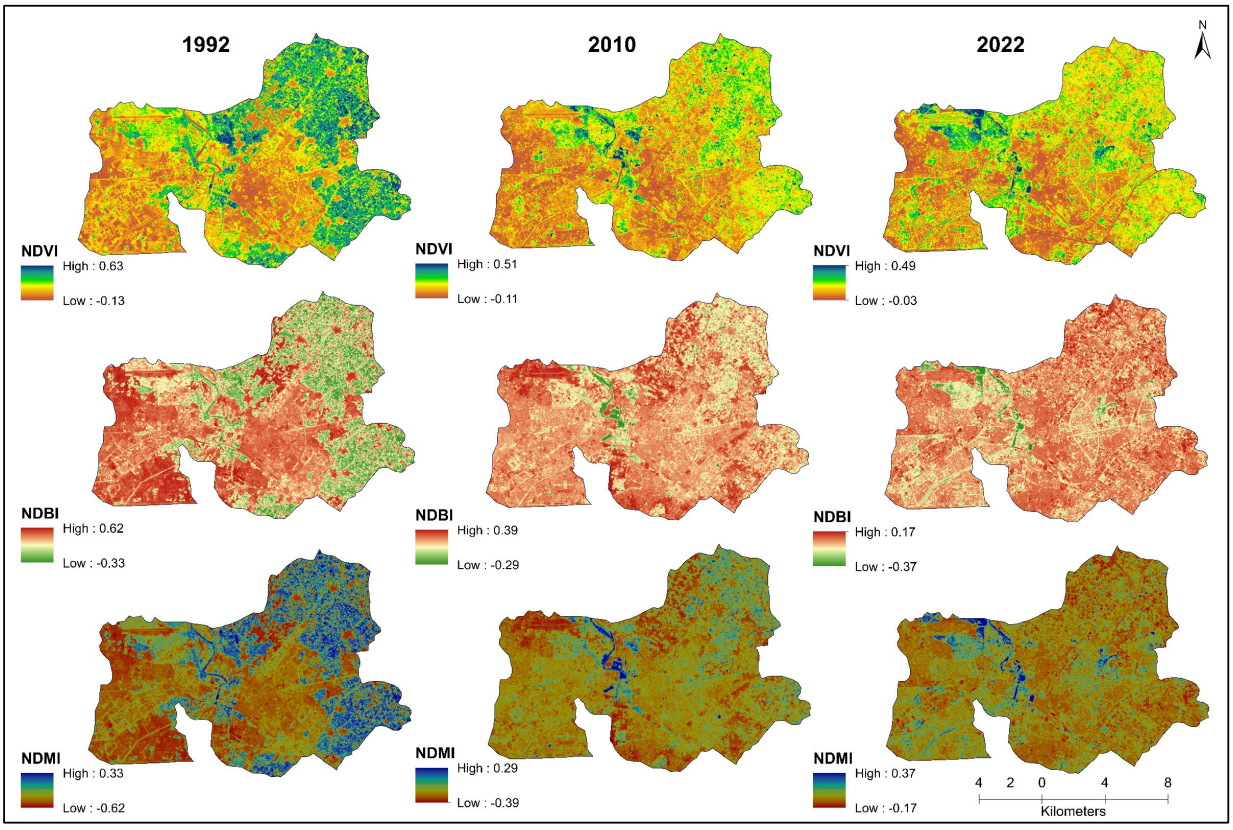

Figure 8. Spatiotemporal analysis of spectral indices– *NDVI*, *NDBI*, and *NDMI*.

Table 6. *NDVI* values in Ghaziabad: 1992–2022.

Date	$NDVI_{Max}$	$NDVI_{Min}$	$NDVI_{Mean}$
16 March 1992	0.63	−0.13	0.21
3 April 2010	0.51	−0.11	0.05
4 April 2022	0.49	0.03	0.17

3.3.2. Spatiotemporal Variation in Normalized Difference Built-Up Index (*NDBI*) in Ghaziabad: 1992–2022

The distribution and variation of *NDBI* values across built-up areas are presented in Table 7 and Figure 8. The *NDBI* values range from − 0.33 to 0.62, − 0.29 to 0.39, and − 0.37 to 0.17 for 1992, 2010, and 2022, respectively. The mean *NDBI* values are presented. The mean *NDBI* values were 0.07 in 1992, 0.17 in 2010, and 0.03 in 2022. The built-up area in Ghaziabad increased over the study period. *NDBI* reached the highest individual value in 1992 (maximum of 0.62), though the mean peaked in 2010. The distribution of values can be seen over the southern, central, southwestern, and some northeastern parts of the research area because the cultivation of crops has been done, and the agricultural lands are vacant, which is why these areas show high values. For 2010, the *NDBI* values are lower than in 2022, but the distribution is mainly in the southern, central, and southeastern parts. The lowest *NDBI* values are obtained for 2022, concentrating primarily in Ghaziabad's south, southeastern, and central areas. This pattern was impacted by industrialization and the expansion of transportation infrastructure during that period. The expansion of built-up areas has had a marked impact on the thermal environment of Ghaziabad, primarily due to the conversion of agricultural land into impervious surfaces.

Table 7. *NDBI* values in Ghaziabad: 1992–2022.

Date	$NDBI_{Max}$	$NDBI_{Min}$	$NDBI_{Mean}$
16 March 1992	0.62	−0.33	0.07
3 April 2010	0.39	−0.29	0.17
4 April 2022	0.17	−0.37	−0.03

3.3.3. Spatiotemporal Variation in Normalized Difference Moisture Index (*NDMI*) in Ghaziabad: 1992–2022

There is a wide range of *NDMI* values and variations during the study period. *NDMI* values fluctuated from −0.62 to 0.33 in 1992, −0.39 to 0.29 in 2010, and −0.17 to 0.37 in 2022, as shown in Table 8 and Figure 8. The average *NDMI* values for 1992, 2010, and 2022 were −0.07, −0.17, and 0.03, respectively. The *NDMI* value in the study area for 1992 was higher than in 2010 but was lower than in 2022. Positive *NDMI* values were primarily observed near the riverine vegetation, while the entire study area showed negative values. The year 2010 had the lowest *NDMI* values, indicating minimal moisture content in the study area, primarily due to the prevalence of exposed open land. Only the Hindon River exhibited positive *NDMI* values, with most of the study area showing negative values for 2010. By 2022, the *NDMI* value had increased, indicating improved moisture conditions due to vegetation and agricultural land. Higher *NDMI* values in 2022 were observed around the river area, as well as in the upper southwestern part, and the eastern and northeastern regions.

Table 8. *NDMI* values in Ghaziabad: 1992–2022.

Date	$NDMI_{Max}$	$NDMI_{Min}$	$NDMI_{Mean}$
16 March 1992	0.33	−0.62	−0.07
3 April 2010	0.29	−0.39	−0.17
4 April 2022	0.37	−0.17	0.03

3.4. The Spatiotemporal Variation in Land Surface Temperature in Ghaziabad: 1992–2022

The spatiotemporal distribution of *LST* in the Ghaziabad area is illustrated in Figure 9 below. According to Table 9, the *LST* values ranged from 14.24 to 28.35 on 16 March 1992, 23.68 to 46.30 on 3 April 2010, and 25.64 to 41.61 on 4 April 2022, as presented in Table 9. The mean *LST* values were 20.81 in 1992, 34.45 in 2010, and 35.01 in 2022. In 1992, the highest *LST* was observed in the southern, western, and southwestern parts of the study area. By 2010, the hot spots had shifted towards the southern, northern, northwestern, and southwestern regions. In 2022, the highest *LST* values were predominantly concentrated in Ghaziabad's southern, southeastern, eastern, and northeastern parts.

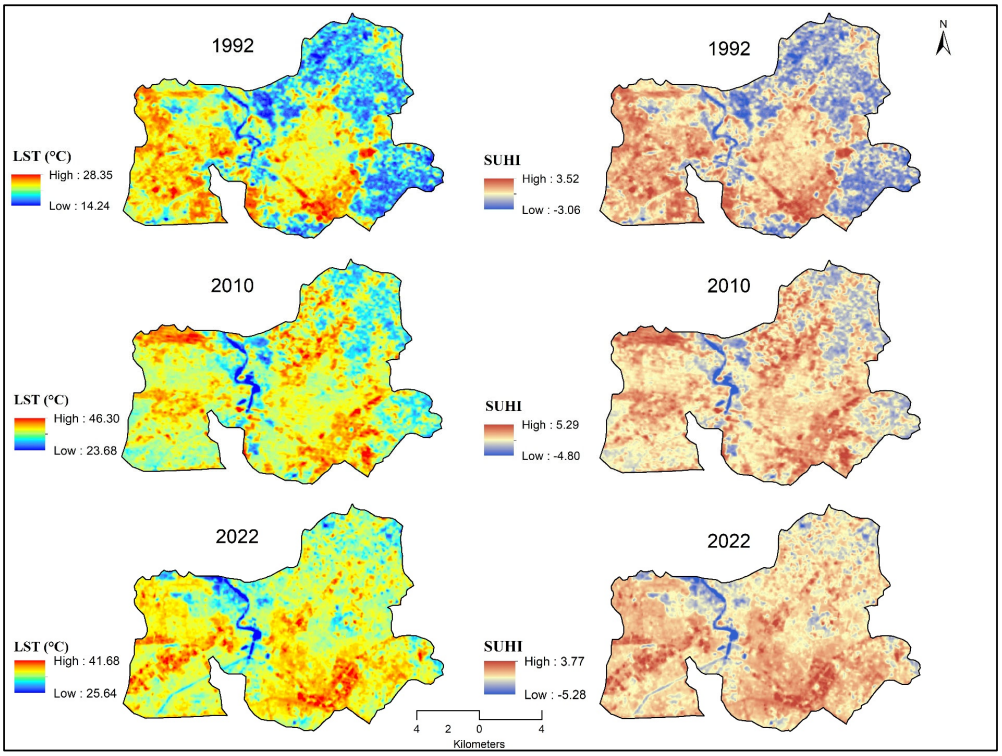

Figure 9. Spatiotemporal variations in *LST* and UHIs in Ghaziabad.

Table 9. *LST* in Ghaziabad.

Date	LST_{Max}	LST_{Min}	LST_{Mean}	LST_{SD}
16 March 1992	28.35	14.24	20.81	2.14
3 April 2010	46.30	23.68	34.45	2.24
4 April 2022	41.61	25.64	35.01	1.77

3.5. The Spatiotemporal Variation in Surface Urban Heat Islands in Ghaziabad: 1992–2022

The temporal and spatial variations in the SUHI intensity across Ghaziabad are shown in Figure 9. The SUHI values ranged from −3.06 to 3.52 in 1992, −4.80 to 5.29 in 2010, and −5.28 to 3.77 in 2022. These ranges indicate a general intensification of SUHI effects over the 30-year study period. By 2022, the highest SUHI values were observed in the central

and southern regions of Ghaziabad, with noticeable SUHI hot spots (high values) also emerging in the eastern and southeastern areas. These elevated SUHI values are mainly due to the concentration of built-up areas and limited vegetation cover in these regions. In contrast, areas dominated by water bodies, vegetation, and agricultural land consistently exhibited lower SUHI values.

Temporally, in 1992 and 2010, high SUHI values were largely associated with exposed open land. Whereas, by 2022, UHIs were primarily concentrated in densely built-up and populated areas. The high-intensity SUHI area progressively expanded, with the central, western, and southwestern regions of Ghaziabad experiencing the highest levels. The urban core of Ghaziabad exhibits progressive SUHI intensification over three decades: from relatively low intensity in 1992, through moderate levels by 2010, to very high intensity by 2022—with central areas experiencing the most severe thermal effects as a direct result of cumulative urban expansion and densification.

3.6. LST Distribution in Different LULC Classes

The spatiotemporal patterns of *LST* across various land use/land cover (LULC) categories from 1992 to 2022 are shown in Figure 10. The analysis indicates a consistent increase in average *LST* across all LULC classes during this period, primarily due to the disproportionate expansion of urban areas compared to green spaces. Notably, the vegetation category experienced an increase in mean *LST*, peaking in 2010, likely associated with the harvesting practices and a limited expansion in vegetation cover. The mean *LST* for built-up areas increased from 21.94 °C in 1992 to 35.64 °C in 2022. For agricultural areas, *LST* increased from 20.21 °C in 1992 to 34.18 °C in 2022. Although the absolute values are significantly lower, water bodies also showed an increasing trend in *LST*. Vegetation and open land displayed inconsistent but overall increasing *LST* patterns over the study period. Specifically, the mean *LST* for open land was 21.18 °C, which rose to 35.28 °C in 2010, followed by a slight decrease to 34.91 °C in 2022. For vegetation, the mean *LST* was 20.05 °C in 1992, increasing to 34.48 °C in 2010, then slightly declining to 33.67 °C in 2022. In summary, all LULC categories exhibited a net increase in *LST* from 1992 to 2022.

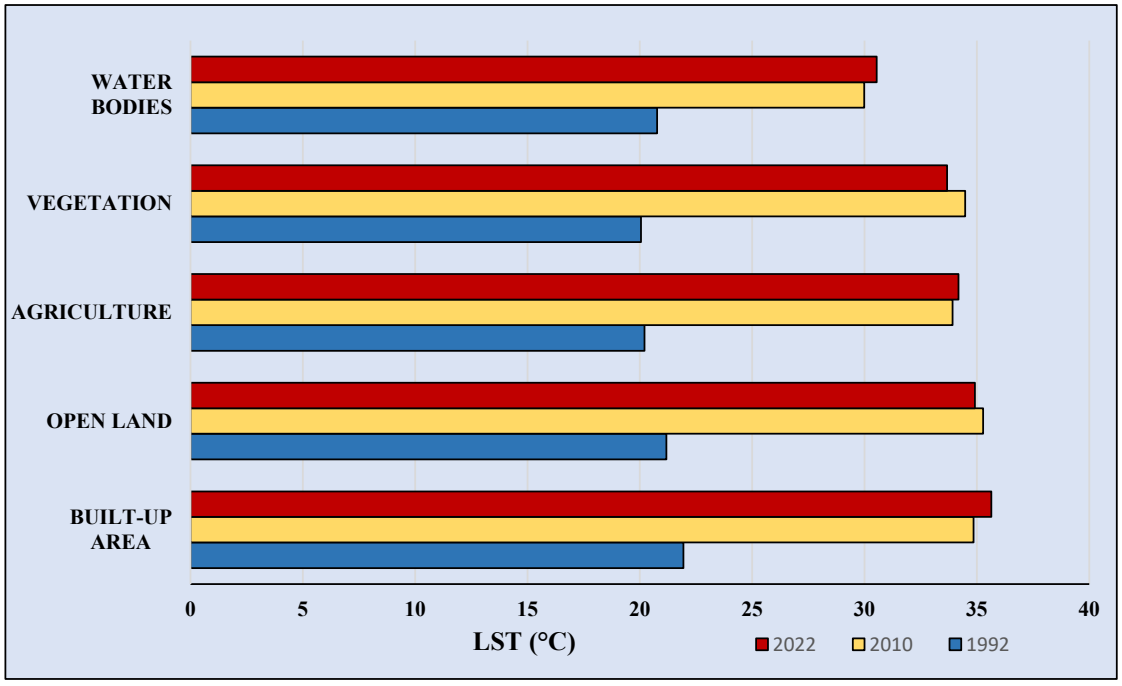

Figure 10. Mean Land Surface Temperature (*LST*) on 16 March 1990, 3 April 2010, and 4 April 2022, by LULC classes in Ghaziabad.

3.7. Urban Thermal Field Variance Index (UTFVI)

The *UTFVI* is a metric used to characterize the urban thermal environment and assess thermal comfort within urban contexts [76]. It is used to quantitatively evaluate the Urban heat island (UHI) phenomenon [77]. As noted by [73], *UTFVI* values are categorized into six thermal ecological levels. For the years 1992, 2010, and 2022, the *UTFVI* values for Ghaziabad were classified into six groups based on thermal comfort levels (Table 10) and are illustrated in Figure 11. The *UTFVI* map shows the spatiotemporal distribution of *UTFVI* extremes (excellent and worst) of thermal ecological assessment. Areas that are significantly warmer than their surroundings exhibit higher *UTFVI* concentrations. The *UTFVI* is widely employed to assess urban ecological quality, particularly emphasizing thermal comfort and UHI intensity. The figure indicates a shift in UHI intensity toward the southeastern region of Ghaziabad. In contrast, the southern region continues to display persistently high thermal stress due to dense built-up areas. Furthermore, the 2022 data show the emergence of smaller patches of middle-to-strongest UHI intensity across Ghaziabad, a pattern not evident in 1992.

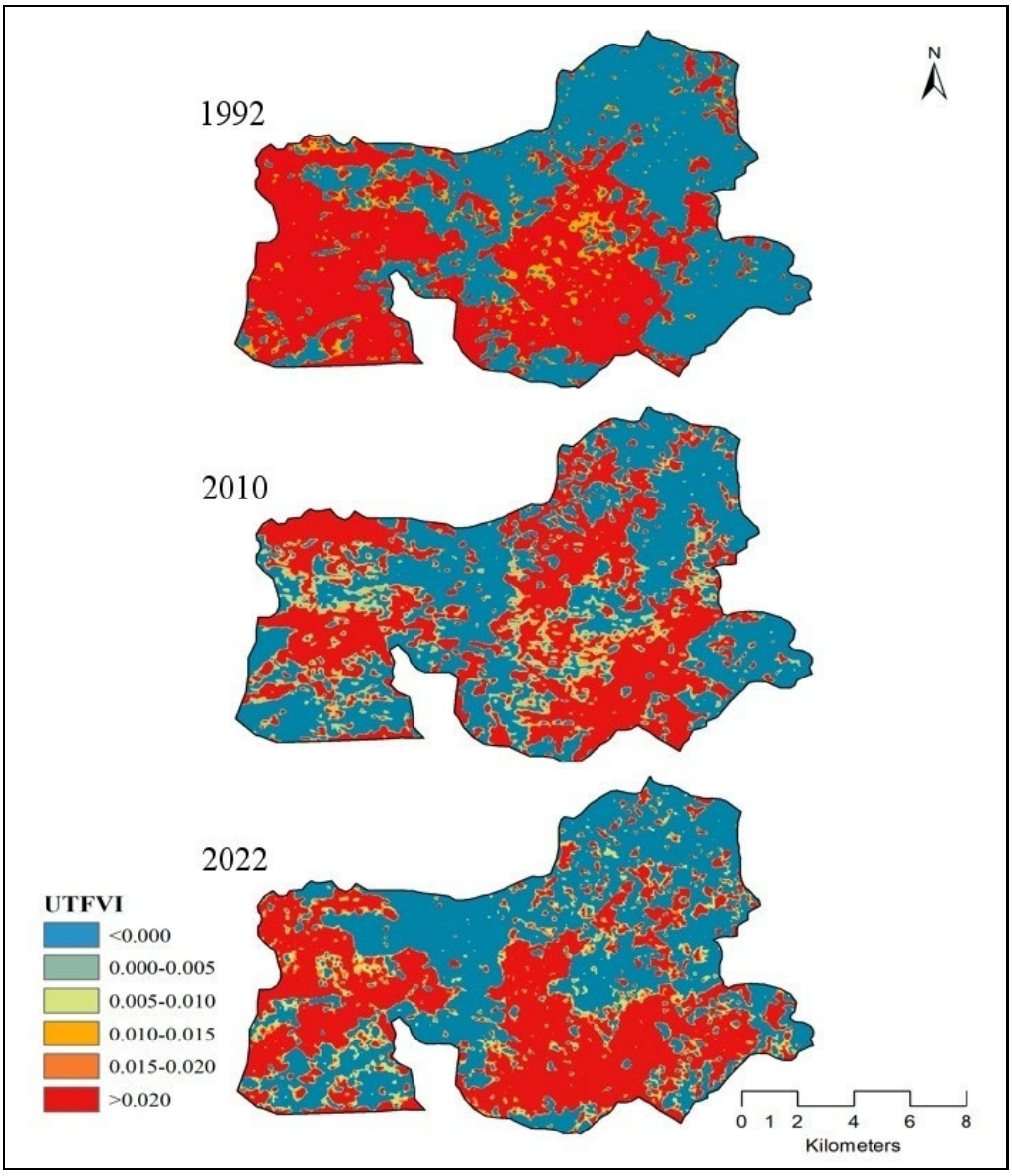

Figure 11. Spatio–temporal variation in the *UTFVI* in Ghaziabad.

Table 10. *UTFVI* thresholds and temporal variation in Ghaziabad.

UTFVI	Urban Heat Island Phenomenon	Ecological Evaluation Index (EEI)	Proportion of Area in Percentage		
			1992	2010	2022
<0	None	Excellent	81.3942	80.4438	83.4669
000–0.005	Weak	Good	0	14.7564	0
0.005–0.010	Middle	Normal	0	0	8.4681
0.015–0.015	Strong	Bad	13.0698	13.608	8.3187
0.015–0.020	Stronger	Worse	0	0	8.4015
>0.020	Strongest	Worst	83.5731	69.2289	69.381

3.8. Identification of Urban Hot Spots (UHSs)

The spatiotemporal variation in *UHSs* across the study area is illustrated in Figure 12. In 1992, small UHS patches were scattered across various parts of Ghaziabad, primarily associated with open land and emerging built-up zones. In 2010, Ghaziabad's eastern and southern regions showed a higher concentration of *UHSs*. There are also some visible spots in the northwestern part of Ghaziabad. These hot spots were still driven by the widespread presence of open land. In 2022, the spatial distribution of *UHSs* shifted more toward the southern and eastern parts of Ghaziabad. At this stage, the primary driver of UHS formation was the high concentration of built-up land, replacing earlier open spaces.

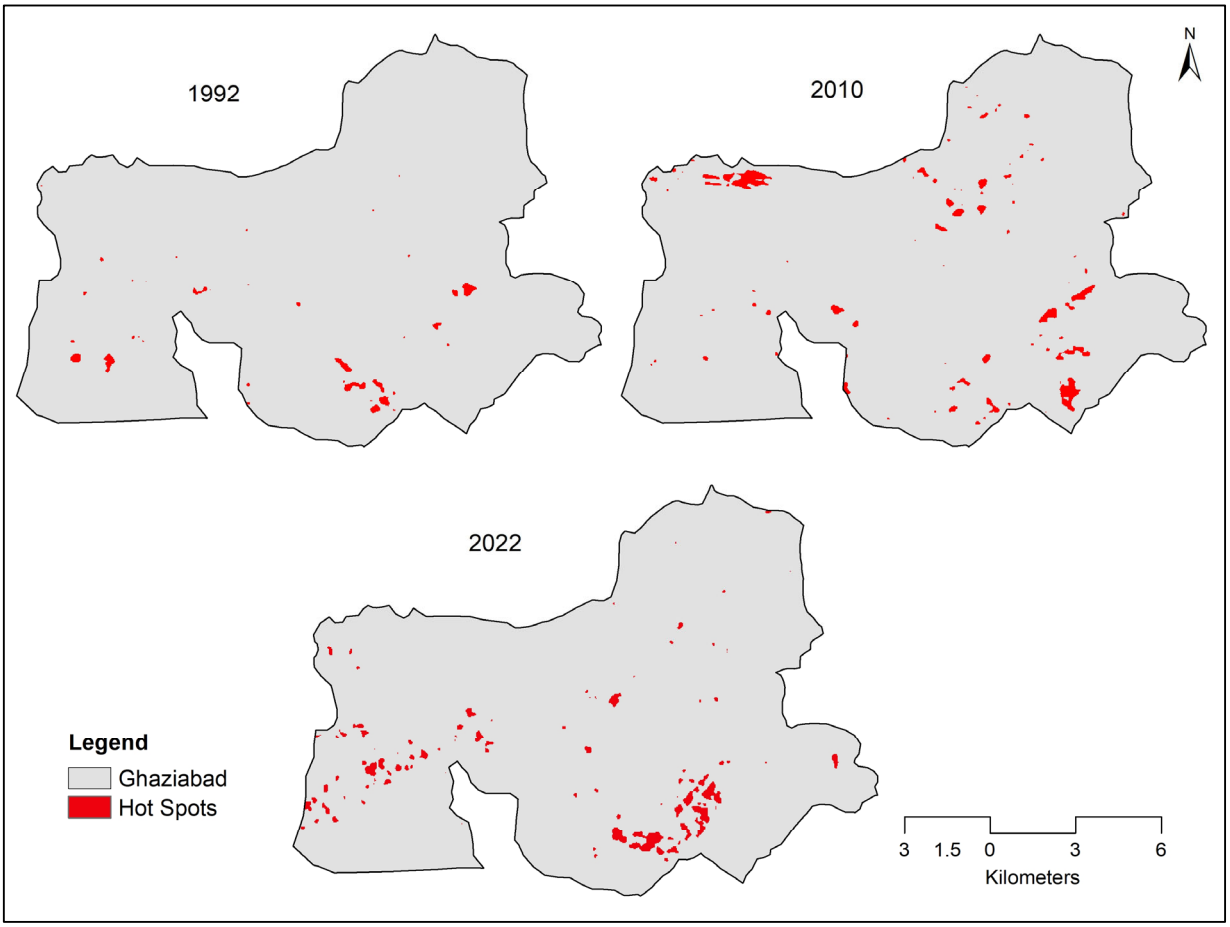

Figure 12. Spatiotemporal variation in urban hot spots (*UHSs*) in Ghaziabad.

4. Exploring the Interconnections of Land Use/Land Cover, LULC Indices, Land Surface Temperature (*LST*), and Urban Heat Islands (UHIs)

Land surface typologies and spatial configurations significantly affect the spatial distribution of UHIs. The pattern and distribution of LULC directly affect UHI intensity [78].

4.1. The Correlation Between LULC and LST

LST is strongly affected by the type and extent of LULC. Changes among various LULC types, especially the expansion of urban areas, exacerbate the UHI effect by increasing the number and distribution of thermal hot spots [30]. *LST* spatial patterns across Ghaziabad were created using Landsat thermal band data (digital numbers 0–255) and classified through the standard deviation method [79]. Table 9 presents the mean *LST* values for each LULC category in the years 1992, 2010, and 2022. The highest average *LST* values were observed in settlement areas, followed by open land, agricultural fields, vegetated areas, and water bodies.

4.2. The Correlation Between Spectral Indices and LST: 1992–2022

The linear relationships between *LST* and the spectral indices *NDVI*, *NDBI*, and *NDMI* used in the study are shown in Figure 13. A strong inverse correlation exists between *NDVI* and *LST*, such that decreases in *NDVI* values are associated with increases in *LST*. Numerous studies confirm that vegetation and *LST* are inversely correlated. For instance, *NDVI* and *LST* values in this study exhibited a negative relationship across all years [80,81]. Higher *NDVI* values are observed in Ghaziabad's northern, southern, and southeastern parts and along the river. However, these areas correspond to regions with dense vegetation and extensive agricultural activity. Conversely, *LST* values were lower in areas dominated by vegetation and agricultural land. The highest *LST* values were observed mainly because of the decline in open land, agricultural land, and vegetation areas. Vegetation reduces thermal radiation and regulates surface temperature [82].

Pearson correlation analysis was employed to examine the relationship between *LST* and *NDVI* using Landsat data for 1992, 2010, and 2022. The analysis showed that areas with higher surface temperatures corresponded to lower *NDVI* values, confirming a negative correlation between vegetation cover and *LST*. The coefficients of determination (R^2) for the correlation between *LST* and *NDVI* were 0.53 in 1992, 0.24 in 2010, and 0.31 in 2022. These results are graphically represented in Figure 13.

LST and *NDBI* have a positive association, which means that the growth of built-up areas causes an increase in *LST*. High *NDBI* values were predominantly concentrated in the central, eastern, and southeastern regions of Ghaziabad. These regions also corresponded with the highest *LST* values, reinforcing the positive association between built-up intensity and surface temperature. This increase in built-up area is primarily driven by industrial development and the conversion of open land, agricultural fields, and vegetated areas into impervious surfaces.

Pearson correlation analysis was conducted to examine the relationship between *LST* and *NDBI*, derived from Landsat data for 1992, 2010, and 2022, respectively. The results indicate higher *NDBI* values in regions with high temperatures, confirming a positive correlation between *LST* and *NDBI*. The correlation coefficients (R^2) were 0.57 for 1992, 0.38 for 2010, and 0.35 for 2022. These trends are illustrated in Figure 13 where the scatter plots show a consistent increasing relationship between *LST* and *NDBI*.

The same correlation analysis assessed the relationship between *NDMI* and *LST*. A negative correlation was observed, indicating that higher surface moisture levels are associated with lower surface temperatures. This relationship is visually depicted in Figure 12.

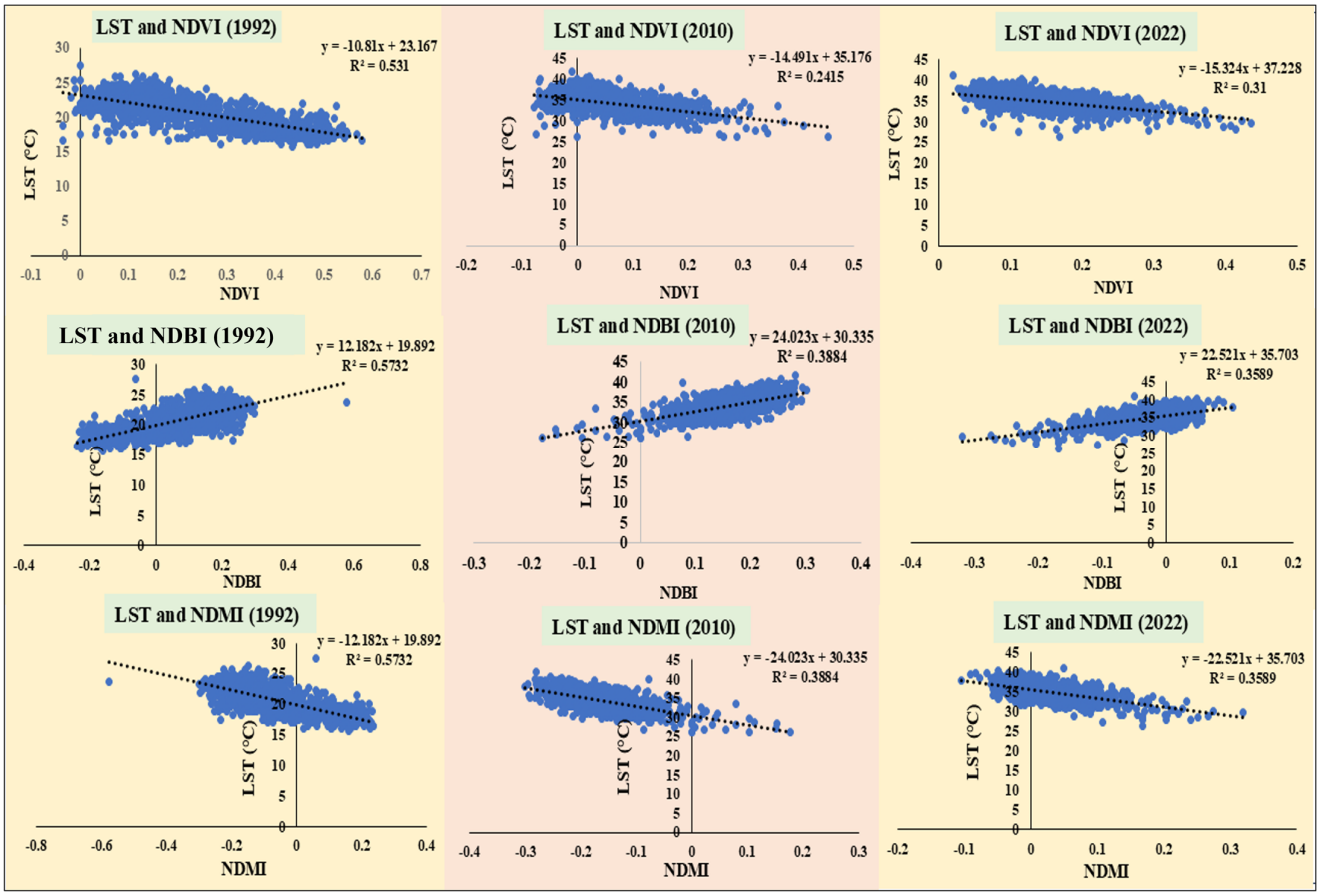

Figure 13. Relationship between *LST* and LULC indices.

5. Discussion

This study analyzed the spatiotemporal dynamics of LULC, their impact on the development of *SUHIs*, and their relationship with urbanization in Ghaziabad between 1992 and 2022, using multi-temporal Landsat datasets. Ghaziabad has undergone dramatic transformations in its LULC pattern, which have notably affected SUHI dynamics [39,83]. The analysis revealed marked spatiotemporal variations in all evaluated land use indices, including *NDVI*, *NDBI*, and *NDMI*. These changes are primarily attributed to urban expansion, increasing built-up areas that retain less moisture than natural surfaces [76,84]. This study explores how temporal shifts in LULC affect *LST* and SUHI patterns. The analysis was focused on detecting LULC changes in Ghaziabad and quantifying the SUHI phenomenon using *LST* derived from GIS and remote sensing. The research addressed the following objectives: (1) to assess the relationship between LULC indices and *LST*; (2) to investigate and track spatiotemporal variations in LULC; (3) to examine the dynamics of *LST* and *SUHIs*; and (4) to identify and analyze urban hot spots (*UHSs*).

Several studies have focused on the spatiotemporal dynamics of LULC [85–89] and their impact on surface urban heat islands [5,23,90–94]. Analysis of LULC changes revealed a significant transformation in land surface composition throughout the study period. This transformation was primarily driven by urban expansion, which reduced vegetation cover, open land, and water bodies [95]. Similar results were observed in a study on Sivas city and also some cities in India, such as Delhi, Noida, Meerut, Mumbai, etc., where vegetated areas declined between 1992 and 2010, followed by an increase from 2010 to 2022 [89,96–98]. *NDVI* values in 1992 showed substantial spatial variability, whereas in 2022, overall *NDVI* values were considerably lower. However, the notable *NDVI* increase observed in specific areas during 2022 may be attributed to plantation initiatives in the Delhi NCR region. *NDBI*

values exhibited notable spatial variation across the study area in 2010, whereas changes were minimal in 1992, reflecting limited urban development in the earlier period. Therefore, to reduce the detrimental impacts of climate change, including UHIs, legislators and urban planners must prioritize integrating green spaces into city planning [99].

The maximum, minimum, and mean values of *LST* in Ghaziabad showed a significant fluctuation for all three datasets used in this study. Temporally, all land use classes have shown a noticeable variation. Built-up area was the category that experienced the highest temperature during both datasets, followed by open land, agriculture, vegetation, and water bodies, except for the data of 3 April 2010. Open land observed higher *LST* than built-up area in 2010 due to exposure of more open hard surfaces, concrete materials, and brick kilns. Similar patterns of vegetative decline and its thermal consequences in cities/urban areas around the world [78]. Studies suggest that reduced (diurnal/daily) temperature variation and rising surface temperatures, characteristic of UHIs, are key indicators of urbanization's contribution to climate change [6].

In Ghaziabad, a significant shift in the SUHI pattern was observed between 1992 and 2010. These changes were primarily linked to barren surfaces and expanding settlements, particularly in the central, southern, and southwestern regions, where built-up land cover was extensive. Like SUHI patterns, urban hot spots (*UHSs*) also exhibited temporal and spatial shifts across Ghaziabad. These areas recorded the highest surface temperatures, largely due to heat-retaining materials such as concrete and asphalt [44]. The development of *UHSs* in Ghaziabad was primarily associated with impervious concrete surfaces and densely settled urban regions. Urban hot spots (*UHSs*) expanded from small, scattered patches in 1992 to a more widespread distribution across Ghaziabad by 2010. However, their highest concentration remained localized in specific built-up zones. However, in 2022, it is clear that inhabited regions have a notably higher proportion of *UHSs*.

This study also assessed how changes in LULC influenced *LST* patterns across the study area. Three geographical indices—the *NDBI*, *NDVI*, and *NDMI*—were used to evaluate their correlations with *LST*. Correlation analysis revealed a significant positive association between *LST* and *NDBI*, indicating that urban expansion contributes directly to increased surface temperatures. The continued expansion of urban features such as concrete and asphalt surfaces results in greater absorption of solar radiation, thereby elevating *LST*. In contrast, both *NDVI* and *NDMI* exhibited negative correlations with *LST*, as higher vegetation and moisture levels help to moderate surface temperatures [66,92].

The intensity of the UHI phenomenon has significantly increased in Indian cities, while urban thermal comfort has declined due to expanding impervious surfaces and the loss of vegetative cover [29,78]. Therefore, to reduce UHI impacts and enhance urban thermal comfort, it is crucial to integrate green infrastructure over barren surfaces and throughout residential and industrial areas. Urban planners and municipal authorities can utilize the findings of this study to inform the spatial planning and distribution of green spaces in Ghaziabad.

6. Conclusions

The current study used different Landsat datasets to evaluate the impact of urbanization on the LULC change of Ghaziabad, as well as the extent to which the observed changes in LULC can be connected to the spatiotemporal pattern of the *LST* and *SUHIs* in Ghaziabad during 1992–2022. Accuracy assessments of the findings demonstrated that over the study period, there was a decline in open land, water bodies, vegetation, and agriculture, and a dramatic increase in built-up areas. The primary catalyst for this expansion of built-up areas is the gradual transition from rural to urban residential communities. The city's central, southern, and southwestern regions have seen the most growth. The findings also

demonstrate the significant influence of all land use indices, including *NDVI*, *NDBI*, and *NDMI* on *SUHIs*. These also have an apparent association with Ghaziabad's *LST*, with built-up area having a more significant influence from 1992 to 2022 than the others. The results obtained also reveal a different pattern of *LST* in Ghaziabad. Between 1992 and 2022, there was a consistent change in the SUHI and *UHSs*. The categories designated as "worse" and "worst" thermal ecological zones in the *UTFVI* showed a notable increase during the study period, signifying a deterioration in the thermal ecological conditions within Ghaziabad from 1992 to 2022. This study indicates that swift urban expansion contributes to the decline of the urban thermal environment in Ghaziabad. Though some regions of Ghaziabad have seen an increase in vegetation in recent years, the central, southern, and southwestern regions of Ghaziabad have experienced a rapid shift due to an unprecedented pace of urbanization.

Considering the study's findings, Ghaziabad has a problem with UHIs and other related issues. As per the findings, locations with high *LST* and UHIs, such as industrial and densely populated areas, can be targeted for mitigation initiatives, including green roofs and lighter-colored surfaces. Determining UHIs is also essential for implementing appropriate mitigation measures, and the government should act immediately to address the urban heat island region by taking the steps needed. To achieve more accurate outcomes, future researchers are advised to consider other factors and locational impacts in their studies on *LST* and UHIs. This study has several limitations, such as using only three time series data; however, more time series data would be ideal for the analysis. If longer-period series data were used in the study, this would produce a better image of the UHI and UHS.

Author Contributions: Conceptualization, M.A. and G.S.; Writing—original draft, Methodology, Data curation, Validation, and Software, M.A.; Visualization and Resources, T.M.U.; Formal analysis, review, and editing, G.S. and R.B.; Supervision, T.M.U. and G.S. All authors have read and agreed to the published version of the manuscript.

Funding: Project no. TKP2021-NKTA-32 has been implemented with the support provided by the National Research, Development and Innovation Fund of Hungary, financed under the TKP2021-NKTA funding scheme.

Data Availability Statement: Data can be made available on reasonable request.

Acknowledgments: The authors are thankful to the United States Geological Survey (USGS) for providing free access to the Landsat data. We also thank both universities for providing a conducive environment for this research.

Conflicts of Interest: All authors declare no conflicts of interest.

References

1. United Nations, Department of Economic and Social Affairs, Population Division. *World Urbanization Prospects: The 2018 Revision*; Online Edition, Data File; United Nations: New York, NY, USA, 2018.
2. Office of the Registrar General & Census Commissioner, India. Census of India 2011. 2011. Available online: https://censusindia.gov.in/ (accessed on 22 April 2024).
3. Franco, S.; Mandla, V.R.; Ram Mohan Rao, K. Trajectory of urban growth and its socioeconomic impact on a rapidly emerging megacity. *J. Urban Plan. Dev.* **2017**, *143*, 04017002. [CrossRef]
4. Zhao, S.; Liu, M.; Tao, M.; Zhou, W.; Lu, X.; Xiong, Y.; Li, F.; Wang, Q. The role of satellite remote sensing in mitigating and adapting to global climate change. *Sci. Total Environ.* **2023**, *904*, 166820. [CrossRef]
5. Grigoras, G.; Uritescu, N. Land use/land cover changes dynamics and their effects on surface urban heat island in Bucharest, Romania. *Int. J. Appl. Earth Obs. Geoinf.* **2019**, *80*, 115–126. [CrossRef]
6. Li, C.; Zhang, N. Analysis of the daytime urban heat island mechanism in East China. *J. Geophys. Res. Atmos.* **2021**, *126*, e2020JD034066. [CrossRef]
7. Grimm, N.B.; Faeth, S.H.; Golubiewski, N.E.; Redman, C.L.; Wu, J.; Bai, X.; Briggs, J.M. Global change and the ecology of cities. *Science* **2008**, *319*, 756–760. [CrossRef] [PubMed]

8. Sheppard, S.R.J. Landscape visualization and climate change: The potential for influencing perceptions and behaviour. *Environ. Sci. Policy* **2005**, *8*, 637–654. [CrossRef]
9. Khorram, S.; Biging, G.; Chrisman, N.; Colby, D.; Congalton, R.G.; Dobson, J.; Ferguson, R. *Accuracy Assessment of Remote Sensing Derived Change Detection*; American Society for Photogrammetry and Remote Sensing: Bethesda, MD, USA, 1999.
10. Turner, B.L.; Lambin, E.F.; Reenberg, A. The emergence of land change science for global environmental change and sustainability. *Proc. Natl. Acad. Sci. USA* **2007**, *104*, 20666–20671. [CrossRef]
11. Berkowicz, R.; Prahm, L.P. Spectral representation of the vertical structure of turbulence in the convective boundary layer. *Q. J. R. Meteorol. Soc.* **1984**, *110*, 35–52. [CrossRef]
12. Deilami, K.; Kamruzzaman, M.; Liu, Y. Urban heat island effect: A systematic review of spatio-temporal factors, data, methods, and mitigation measures. *Int. J. Appl. Earth Obs. Geoinf.* **2018**, *67*, 30–42. [CrossRef]
13. El-Hattab, M.; Amany, S.M.; Lamia, G.E. Monitoring and assessment of urban heat islands over the Southern region of Cairo Governorate, Egypt. *Egypt. J. Remote Sens. Space Sci.* **2018**, *21*, 311–323. [CrossRef]
14. Shaban, A.; Kourtit, K.; Nijkamp, P. India's urban system: Sustainability and imbalanced growth of cities. *Sustainability* **2020**, *12*, 2941. [CrossRef]
15. Sarkar, R. Urbanization in India before and after the economic reforms: What does the census data reveal? *J. Asian Afr. Stud.* **2019**, *54*, 1213–1226. [CrossRef]
16. Brown, D.G.; Pijanowski, B.C.; Duh, J.D. Modeling the relationships between land use and land cover on private lands in the Upper Midwest, USA. *J. Environ. Manag.* **2000**, *59*, 247–263. [CrossRef]
17. Manoli, G.; Fatichi, S.; Schläpfer, M.; Yu, K.; Crowther, T.W.; Meili, N.; Burlando, P.; Katul, G.G.; Bou-Zeid, E. Magnitude of urban heat islands largely explained by climate and population. *Nature* **2019**, *573*, 55–60. [CrossRef] [PubMed]
18. Zhao, L.; Lee, X.; Smith, R.B.; Oleson, K. Strong contributions of local background climate to urban heat islands. *Nature* **2014**, *511*, 216–219. [CrossRef] [PubMed]
19. Sajikumar, N.; Remya, R.S. Impact of land cover and land use change on runoff characteristics. *J. Environ. Manag.* **2015**, *161*, 460–468. [CrossRef]
20. Sarif, M.O.; Gupta, R.D. Modelling of trajectories in urban sprawl types and their dynamics (1988–2018): A case study of Prayagraj City (India). *Arab. J. Geosci.* **2021**, *14*, 1347. [CrossRef]
21. Shahfahad, R.; Rihan, M.; Naikoo, M.W.; Ali, M.A.; Usmani, T.M.; Rahman, A. Urban heat island dynamics in response to land-use/land-cover change in the coastal city of Mumbai. *J. Indian Soc. Remote Sens.* **2021**, *49*, 2227–2247. [CrossRef]
22. Naikoo, M.W.; Islam, A.R.M.T.; Mallick, J.; Rahman, A. Land use/land cover change and its impact on surface urban heat island and urban thermal comfort in a metropolitan city. *Urban Clim.* **2022**, *41*, 101052. [CrossRef]
23. Trolle, D.; Nielsen, A.; Andersen, H.E.; Thodsen, H.; Olesen, J.E.; Børgesen, C.D.; Refsgaard, J.C.; Sonnenborg, T.O.; Karlsson, I.B.; Christensen, J.P.; et al. Effects of changes in land use and climate on aquatic ecosystems: Coupling of models and decomposition of uncertainties. *Sci. Total Environ.* **2019**, *657*, 627–633. [CrossRef]
24. Fu, Y.; Li, J.; Weng, Q.; Zheng, Q.; Li, L.; Dai, S.; Guo, B. Characterizing the spatial pattern of annual urban growth by using time series Landsat imagery. *Sci. Total Environ.* **2019**, *666*, 274–284. [CrossRef]
25. Fu, P.; Weng, Q. Variability in annual temperature cycle in the urban areas of the United States as revealed by MODIS imagery. *ISPRS J. Photogramm. Remote Sens.* **2018**, *146*, 65–73. [CrossRef]
26. Roth, M. Understanding urban heat islands. In *The Routledge Handbook of Urban Ecology*; Routledge: Abingdon-on-Thames, UK, 2020; pp. 142–154.
27. Oke, T.R. The heat island of the urban boundary layer: Characteristics, causes and effects. In *Wind Climate in Cities*; Springer: Dordrecht, The Netherlands, 1995; pp. 81–107.
28. Karimi, A.; Mohammad, P.; Gachkar, S.; Gachkar, D.; García-Martínez, A.; Moreno-Rangel, D.; Brown, R.D. Surface urban heat island assessment of a cold desert city: A case study over the Isfahan Metropolitan Area of Iran. *Atmosphere* **2021**, *12*, 1368. [CrossRef]
29. Pandey, A.; Brauer, M.; Cropper, M.L.; Balakrishnan, K.; Mathur, P.; Dey, S.; Turkgulu, B.; Kumar, G.A.; Khare, M.; Beig, G.; et al. Health and economic impact of air pollution in the states of India: The Global Burden of Disease Study 2019. *Lancet Planet. Health* **2021**, *5*, e25–e38. [CrossRef] [PubMed]
30. Tran, H.; Uchihama, D.; Ochi, S.; Yasuoka, Y. Assessment with satellite data of the urban heat island effects in Asian mega cities. *Int. J. Appl. Earth Obs. Geoinf.* **2006**, *8*, 34–48. [CrossRef]
31. Yuan, F.; Bauer, M.E. Comparison of impervious surface area and normalized difference vegetation index as indicators of surface urban heat island effects in Landsat imagery. *Remote Sens. Environ.* **2007**, *106*, 375–386. [CrossRef]
32. Xiao, H.; Kopecká, M.; Guo, S.; Guan, Y.; Cai, D.; Zhang, C.; Zhang, X.; Yao, W. Responses of urban land surface temperature on land cover: A comparative study of Vienna and Madrid. *Sustainability* **2018**, *10*, 260. [CrossRef]
33. Mentaschi, L.; Duveiller, G.; Zulian, G.; Corbane, C.; Pesaresi, M.; Maes, J.; Feyen, L. Global long-term mapping of surface temperature shows intensified intra-city urban heat island extremes. *Glob. Environ. Change* **2022**, *72*, 102441. [CrossRef]

34. Marcotullio, P.J.; Keßler, C.; Quintero Gonzalez, R.; Schmeltz, M. Urban growth and heat in tropical climates. *Front. Ecol. Evol.* **2021**, *9*, 616626. [CrossRef]
35. Lu, X.; Lin, C.; Li, W.; Chen, Y.; Huang, Y.; Fung, J.C.; Lau, A.K. Analysis of the adverse health effects of PM2.5 from 2001 to 2017 in China and the role of urbanization in aggravating the health burden. *Sci. Total Environ.* **2019**, *652*, 683–695. [CrossRef]
36. Reba, M.; Seto, K.C. A systematic review and assessment of algorithms to detect, characterize, and monitor urban land change. *Remote Sens. Environ.* **2020**, *242*, 111739. [CrossRef]
37. Jenerette, G.D.; Harlan, S.L.; Buyantuev, A.; Stefanov, W.L.; Declet-Barreto, J.; Ruddell, B.L.; Li, X. Micro-scale urban surface temperatures are related to land-cover features and residential heat related health impacts in Phoenix, AZ USA. *Landsc. Ecol.* **2016**, *31*, 745–760. [CrossRef]
38. Jamal, S.; Saqib, M.; Ahmad, W.S.; Ahmad, M.; Ali, M.A.; Ali, M.B. Unraveling the complexities of land transformation and its impact on urban sustainability through land surface temperature analysis. *Appl. Geomat.* **2023**, *15*, 719–741. [CrossRef]
39. Mallick, J.; Rahman, A.; Singh, C.K. Modeling urban heat islands in heterogeneous land surface and its correlation with impervious surface area by using night-time ASTER satellite data in highly urbanizing city, Delhi-India. *Adv. Space Res.* **2013**, *52*, 639–655. [CrossRef]
40. Shahfahad Bindajam, A.A.; Naikoo, M.W.; Horo, J.P.; Mallick, J.; Rihan, M.; Rahman, A. Response of soil moisture and vegetation conditions in seasonal variation of land surface temperature and surface urban heat island intensity in sub-tropical semi-arid cities. *Theor. Appl. Climatol.* **2023**, *153*, 367–395. [CrossRef]
41. Yang, J.; Wang, Y.; Xiao, X.; Jin, C.; Xia, J.C.; Li, X. Spatial differentiation of urban wind and thermal environment in different grid sizes. *Urban Clim.* **2019**, *28*, 100458. [CrossRef]
42. Gasparrini, A.; Guo, Y.; Sera, F.; Vicedo-Cabrera, A.M.; Huber, V.; Tong, S.; Armstrong, B. Projections of temperature-related excess mortality under climate change scenarios. *Lancet Planet. Health* **2017**, *1*, e360–e367. [CrossRef]
43. *Addis Ababa Action Agenda*; A/CONF.227/L.1; United Nations: New York, NY, USA, 2015.
44. Lopez, J.M.R.; Heider, K.; Scheffran, J. Frontiers of urbanization: Identifying and explaining urbanization hot spots in the south of Mexico City using human and remote sensing. *Appl. Geogr.* **2017**, *79*, 1–10. [CrossRef]
45. Guha, S.; Govil, H.; Dey, A.; Gill, N. Analytical study of land surface temperature with *NDVI* and *NDBI* using Landsat 8 OLI and TIRS data in Florence and Naples city, Italy. *Eur. J. Remote Sens.* **2018**, *51*, 667–678. [CrossRef]
46. Kumar, K.S.; Bhaskar, P.U.; Padmakumari, K. Estimation of land surface temperature to study urban heat island effect using Landsat ETM+ image. *Int. J. Eng. Sci. Technol.* **2012**, *4*, 771–778.
47. Das, S.; Sarkar, R. Spatiotemporal change detection analysis of land cover and land use using multi-temporal remote sensed imagery and landscape metrics: A sub-catchment level case study of the Bhagirathi-Hugli River, West Bengal, India. In *IOP Conference Series: Earth and Environmental Science*; IOP Publishing: Bristol, UK, 2023; Volume 1164, p. 012003.
48. Shalaby, A.; Tateishi, R. Remote sensing and GIS for mapping and monitoring land cover and land-use changes in the Northwestern coastal zone of Egypt. *Appl. Geogr.* **2007**, *27*, 28–41. [CrossRef]
49. Karakus, C.B.; Kavak, K.S.; Cerit, O. Determination of variations in land cover and land use by remote sensing and geographic information systems around the city of Sivas (Turkey). *Fresenius Environ. Bull.* **2014**, *23*, 667–677.
50. Ozesmi, S.L.; Bauer, M.E. Satellite remote sensing of wetlands. *Wetl. Ecol. Manag.* **2002**, *10*, 381–402. [CrossRef]
51. GEOG, Department of Geography, Penn State College of Earth and Mineral Sciences. Remote Sensing Analysis and Applications. 2016. Available online: https://www.e-education.psu.edu/geog883/node/524 (accessed on 25 June 2018).
52. Lu, D.; Weng, Q. A survey of image classification methods and techniques for improving classification performance. *Int. J. Remote Sens.* **2007**, *28*, 823–870. [CrossRef]
53. Wondrade, N.; Dick, Q.B.; Tveite, H. GIS-based mapping of land cover changes utilizing multi-temporal remotely sensed image data in Lake Hawassa watershed, Ethiopia. *Environ. Monit. Assess.* **2014**, *186*, 1765–1780. [CrossRef]
54. Yuan, F.; Sawaya, K.E.; Loeffelholz, B.C.; Bauer, M.E. Land cover classification and change analysis of the Twin Cities (Minnesota) metropolitan area by multitemporal Landsat remote sensing. *Remote Sens. Environ.* **2005**, *98*, 317–328. [CrossRef]
55. Xiao, H.; Weng, Q. The impact of land use and land cover changes on land surface temperature in a karst area of China. *J. Environ. Manag.* **2007**, *85*, 245–257. [CrossRef]
56. Ji, X.; Niu, X. The attribute accuracy assessment of land cover data in the national geography conditions survey. *ISPRS Ann. Photogramm. Remote Sens. Spat. Inf. Sci.* **2014**, *2*, 35–40.
57. Gandhi, G.M.; Parthiban, S.; Thummalu, N.; Christy, A. *NDVI*: Vegetation change detection using remote sensing and GIS—A case study of Vellore District. *Procedia Comput. Sci.* **2015**, *57*, 1199–1210. [CrossRef]
58. Silleos, N.G.; Alexandridis, T.K.; Gitas, I.Z.; Perakis, K. Vegetation indices: Advances made in biomass estimation and vegetation monitoring in the last 30 years. *Geocarto Int.* **2006**, *21*, 21–28. [CrossRef]
59. Kriegler, F.J.; Malila, W.A.; Nalepka, R.F.; Richardson, W. Preprocessing transformations and their effects on multispectral recognition. In Proceedings of the Sixth International Symposium on Remote Sensing of Environment, University of Michigan, Ann Arbor, MI, USA, 13–16 October 1969; pp. 97–131.

60. Zha, Y.; Gao, J.; Ni, S. Use of normalized difference built-up index in automatically mapping urban areas from TM imagery. *Int. J. Remote Sens.* **2003**, *24*, 583–594. [CrossRef]
61. Jin, S.; Sader, S.A. Comparison of time series tasseled cap wetness and the normalized difference moisture index in detecting forest disturbances. *Remote Sens. Environ.* **2005**, *94*, 364–372. [CrossRef]
62. Fan, C.; Myint, S.W.; Kaplan, S.; Middel, A.; Zheng, B.; Rahman, A.; Blumberg, D.G. Understanding the impact of urbanization on surface urban heat islands—A longitudinal analysis of the oasis effect in subtropical desert cities. *Remote Sens.* **2017**, *9*, 672. [CrossRef]
63. Chander, G.; Markham, B.L.; Helder, D.L. Summary of current radiometric calibration coefficients for Landsat MSS, TM, ETM+, and EO-1 ALI sensors. *Remote Sens. Environ.* **2009**, *113*, 893–903. [CrossRef]
64. Santamouris, M.; Synnefa, A.; Karlessi, T. Using advanced cool materials in the urban built environment to mitigate heat islands and improve thermal comfort conditions. *Sol. Energy* **2011**, *85*, 3085–3102. [CrossRef]
65. Mirzaei, P.A.; Haghighat, F. Approaches to study urban heat island–abilities and limitations. *Build. Environ.* **2010**, *45*, 2192–2201. [CrossRef]
66. Yao, R.; Wang, L.; Huang, X.; Zhang, W.; Li, J.; Niu, Z. Interannual variations in surface urban heat island intensity and associated drivers in China. *J. Environ. Manag.* **2018**, *222*, 86–94. [CrossRef]
67. Weng, Q.; Firozjaei, M.K.; Kiavarz, M.; Alavipanah, S.K.; Hamzeh, S. Normalizing land surface temperature for environmental parameters in mountainous and urban areas of a cold semi-arid climate. *Sci. Total Environ.* **2019**, *650*, 515–529. [CrossRef]
68. Das, P.; Vamsi, K.S.; Zhenke, Z. Decadal variation of the land surface temperatures (*LST*) and urban heat island (UHI) over Kolkata City projected using MODIS and ERA-interim datasets. *Aerosol Sci. Eng.* **2020**, *4*, 200–209. [CrossRef]
69. Dewan, A.; Kiselev, G.; Botje, D.; Mahmud, G.I.; Bhuian, M.H.; Hassan, Q.K. Surface urban heat island intensity in five major cities of Bangladesh: Patterns, drivers and trends. *Sustain. Cities Soc.* **2021**, *71*, 102926. [CrossRef]
70. Jiang, Y.; Lin, W. A comparative analysis of retrieval algorithms of land surface temperature from Landsat-8 data: A case study of Shanghai, China. *Int. J. Environ. Res. Public Health* **2021**, *18*, 5659. [CrossRef] [PubMed]
71. Reddy, S.N.; Manikiam, B.; Jeevalakshmi, D. Land Surface Temperature Retrieval from LANDSAT data using Emissivity Estimation. *Int. J. Appl. Eng. Res.* **2017**, *12*, 9679–9687.
72. Liu, L.; Zhang, Y. Urban heat island analysis using the Landsat TM data and ASTER data: A case study in Hong Kong. *Remote Sens.* **2011**, *3*, 1535–1552. [CrossRef]
73. Zhang, Y. Land surface temperature retrieval from CBERS-02 IRMSS thermal infrared data and its applications in quantitative analysis of urban heat island effect. *J. Remote Sens.* **2006**, *10*, 789–797.
74. Rahman, A.; Kumar, S.; Fazal, S.; Siddiqui, M.A. Assessment of land use/land cover change in the North-West District of Delhi using remote sensing and GIS techniques. *J. Indian Soc. Remote Sens.* **2012**, *40*, 689–697. [CrossRef]
75. Census of India. Primary Census Abstract: Uttar Pradesh, Office of Registrar General and Census Commissioner, New Delhi. 2011. Available online: http://www.censusindia.gov.in/2011census/hlo/pca/PCA_Data_UP.html (accessed on 22 January 2017).
76. Maithani, S.; Nautiyal, G.; Sharma, A. Investigating the effect of lockdown during COVID-19 on land surface temperature: Study of Dehradun city, India. *J. Indian Soc. Remote Sens.* **2020**, *48*, 1297–1311. [CrossRef]
77. Renard, F.; Alonso, L.; Fitts, Y.; Hadjiosif, A.; Comby, J. Evaluation of the effect of urban redevelopment on surface urban heat islands. *Remote Sens.* **2019**, *11*, 299. [CrossRef]
78. Pramanik, S.; Punia, M. Land use/land cover change and surface urban heat island intensity: Source–sink landscape-based study in Delhi, India. *Environ. Dev. Sustain.* **2020**, *22*, 7331–7356. [CrossRef]
79. Weng, Q.; Lu, D.; Schubring, J. Estimation of land surface temperature–vegetation abundance relationship for urban heat island studies. *Remote Sens. Environ.* **2004**, *89*, 467–483. [CrossRef]
80. Li, H.; Sun, D.; Yu, Y.; Wang, H.; Liu, Y.; Liu, Q.; Du, Y.; Wang, H.; Cao, B. Evaluation of the VIIRS and MODIS *LST* products in an arid area of Northwest China. *Remote Sens. Environ.* **2014**, *142*, 111–121. [CrossRef]
81. Kaplan, G.; Avdan, U.; Avdan, Z.Y. Urban heat island analysis using the landsat 8 satellite data: A case study in Skopje, Macedonia. *Proceedings* **2018**, *2*, 358. [CrossRef]
82. Chakraborty, S.D.; Kant, Y.; Bharath, B.D. Study of land surface temperature in delhi city to managing the thermal effect on urban developments. *Int. J. Adv. Sci. Tech. Res.* **2014**, *4*, 439–450.
83. Sultana, S.; Satyanarayana, A.N.V. Urban heat island intensity during winter over metropolitan cities of India using remote-sensing techniques: Impact of urbanization. *Int. J. Remote Sens.* **2018**, *39*, 6692–6730. [CrossRef]
84. Mishra, K.; Garg, R.D. Assessing variations in land cover-land use and surface temperature dynamics for Dehradun, India, using multi-time and multi-sensor Landsat data. *Environ. Monit. Assess.* **2023**, *195*, 373. [CrossRef]
85. Turner, B.L.; Skole, D.; Sanderson, S.; Fischer, G.; Fresco, L.; Leemans, R. Land-Use and Land-Cover Change: Science/Research Plan. 1995. Available online: https://pure.iiasa.ac.at/id/eprint/4402/ (accessed on 22 January 2017).
86. Lambin, E.F.; Geist, H.J.; Lepers, E. Dynamics of land-use and land-cover change in tropical regions. *Annu. Rev. Environ. Resour.* **2003**, *28*, 205–241. [CrossRef]

87. Souza, C.M., Jr.; Shimbo, J.Z.; Rosa, M.R.; Parente, L.L.; Alencar, A.A.; Rudorff, B.F.T.; Hasenack, H.; Matsumoto, M.; Ferreira, L.G.; Souza-Filho, P.W.M.; et al. Reconstructing three decades of land use and land cover changes in Brazilian biomes with Landsat archive and Earth Engine. *Remote Sens.* **2020**, *12*, 2735. [CrossRef]
88. Chen, Y.; Yang, J.; Yu, W.; Ren, J.; Xiao, X.; Xia, J.C. Relationship between urban spatial form and seasonal land surface temperature under different grid scales. *Sustain. Cities Soc.* **2023**, *89*, 104374. [CrossRef]
89. Talukdar, S.; Rihan, M.; Hang, H.T.; Bhaskaran, S.; Rahman, A. Modelling urban heat island (UHI) and thermal field variation and their relationship with land use indices over Delhi and Mumbai metro cities. *Environ. Dev. Sustain.* **2022**, *24*, 3762–3790. [CrossRef]
90. Dissanayake, D.; Morimoto, T.; Ranagalage, M.; Murayama, Y. Land-use/land-cover changes and their impact on surface urban heat islands: Case study of Kandy City, Sri Lanka. *Climate* **2019**, *7*, 99. [CrossRef]
91. Bokaie, M.; Zarkesh, M.K.; Arasteh, P.D.; Hosseini, A. Assessment of urban heat island based on the relationship between land surface temperature and land use/land cover in Tehran. *Sustain. Cities Soc.* **2016**, *23*, 94–104. [CrossRef]
92. Zhou, W.; Qian, Y.; Li, X.; Li, W.; Han, L. Relationships between land cover and the surface urban heat island: Seasonal variability and effects of spatial and thematic resolution of land cover data on predicting land surface temperatures. *Landsc. Ecol.* **2014**, *29*, 153–167. [CrossRef]
93. Silva, J.S.; Da Silva, R.M.; Santos, C.A.G. Spatiotemporal impact of land use/land cover changes on urban heat islands: A case study of Paço do Lumiar, Brazil. *Build. Environ.* **2018**, *136*, 279–292. [CrossRef]
94. Lo, C.P.; Quattrochi, D.A. Land-use and land-cover change, urban heat island phenomenon, and health implications. *Photogramm. Eng. Remote Sens.* **2003**, *69*, 1053–1063. [CrossRef]
95. Kanga, S.; Singh, S.K.; Meraj, G.; Kumar, A.; Parveen, R.; Kranjčić, N.; Đurin, B. Assessment of the impact of urbanization on geoenvironmental settings using geospatial techniques: A study of Panchkula District, Haryana. *Geographies* **2022**, *2*, 1–10. [CrossRef]
96. Karakuş, C.B. The impact of land use/land cover (LULC) changes on land surface temperature in Sivas City Center and its surroundings and assessment of Urban Heat Island. *Asia-Pac. J. Atmos. Sci.* **2019**, *55*, 669–684. [CrossRef]
97. Sharma, R.; Pradhan, L.; Kumari, M.; Bhattacharya, P. Assessing urban heat islands and thermal comfort in Noida City using geospatial technology. *Urban Clim.* **2021**, *35*, 100751. [CrossRef]
98. Joshi, K.; Kumari, M.; Mishra, V.N.; Prasad, R.; Zhran, M. Geoinformatics based evaluation of heat mitigation strategies through urban green spaces in a rapidly growing city of India: Implications for urban resilience. *Theor. Appl. Climatol.* **2025**, *156*, 1–24. [CrossRef]
99. Rahaman, S.; Jahangir, S.; Haque, M.S.; Chen, R.; Kumar, P. Spatio-temporal changes of green spaces and their impact on urban environment of Mumbai. *Environ. Dev. Sustain.* **2020**, *23*, 6481–6501. [CrossRef]

Disclaimer/Publisher's Note: The statements, opinions and data contained in all publications are solely those of the individual author(s) and contributor(s) and not of MDPI and/or the editor(s). MDPI and/or the editor(s) disclaim responsibility for any injury to people or property resulting from any ideas, methods, instructions or products referred to in the content.